Chapter 5

Applied Catalysis A, General 643 (2022) 118767

Contents lists available at ScienceDirect

Applied Catalysis A, General

journal homepage: www.elsevier.com/locate/apcata

An avenue to Chan-Lam *N*-arylation by Cu(0) nanoparticles immobilized graphitic carbon-nitride oxide surface

Rakhee Saikia [a], Purna K. Boruah [b], Sahid Mostak Ahmed [a], Manash R. Das [b,c], Ashim J. Thakur [a], Utpal Bora [a,*]

[a] Department of Chemical Sciences, Tezpur University, Napaam, Tezpur, Assam 784028, India
[b] Advanced Materials Group, Materials Sciences and Technology Division, CSIR-North East Institute of Science and Technology, Jorhat 785006 Assam, India
[c] Academy of Scientific and Innovative Research (AcSIR), Ghaziabad 201002, India

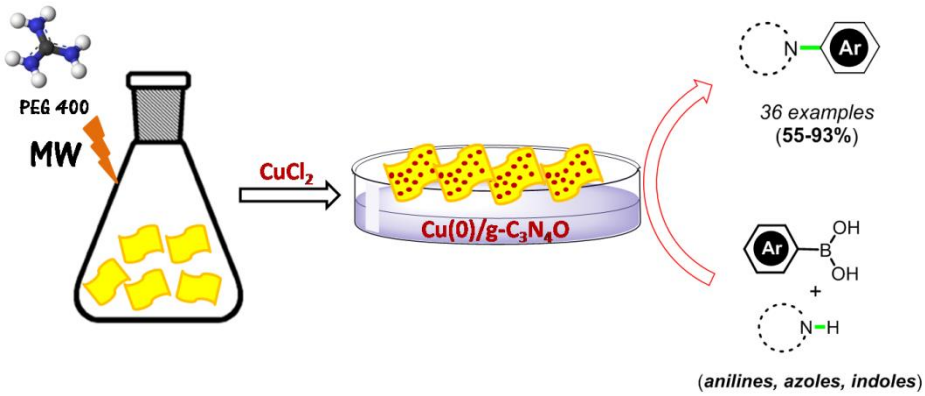

ABSTRACT: This chapter reports the immobilization of Cu(0) nanoparticles (NPs) with an average size of 7-8 nm on a template-free carbon-nitride oxide surface (g-C_3N_4O) in water medium. The heterogeneous surface containing Cu(0) NPs offers Lewis basic sites, which facilitate Chan-Lam *N*-arylation of anilines, azoles and indoles with phenylboronic acids. Moderate to excellent yields (55-93%) of synthetically and pharmaceutically important *N*–arylanilines, *N*–aryl–1*H*–imidazoles, *N*–aryl–1*H*–benzimidazoles and *N*–aryl–1*H*–indoles are obtained. The reaction takes place under heterogeneous catalysis and the catalyst can be reused up to five catalytic cycles of the reaction. The stability of Cu(0) on the g-C_3N_4O surface, utilization of greener solvents for syntheses and extension of scope of Chan-Lam cross-coupling reaction through the introduction of Cu(0) NPs catalysis are some of the significant achievements of this work.

Chapter 5

5. Copper (zero) nanoparticles in Chan-Lam cross-coupling reaction

5.1 *Introduction*

The pioneering discovery of a mild Cu-mediated cross-coupling between arylboronic acids and −NH, −OH or −SH nucleophiles, independently reported by Chan [1], Evans [2] and Lam [3-4] led to rapid growth in C−N bond transformation. Although Ullmann/Goldberg reactions are step economical in terms of the use of aryl halides as the arylating partner, they heavily rely on “expensive metal catalysis−high temperature” reaction conditions. On the other hand, Chan-Lam cross-coupling requires “ambient temperature catalysis−open flask” conditions. This powerful nucleophile-nucleophile (oxidative) cross-coupling employs “air stable” boronic acids as the arylating partner and displays wide substrate scope with a much easier “open-flask” approach (ambient temperature, mild base and run in air) [5-9]. Though the utilization of arylboronic acids, primarily synthesized from aryl halides may be a matter of concern, recent reports have suggested that arylboronic acids can be prepared directly through C-H borylation of arenes [10,11]. Apart from aryl amines, the scope of the reaction also extends to other heteroatom nucleophiles like alkyl amines [12], alcohols [13], ammonia [14], guanidines [15,16], hydrazines [17,18], sulphonamides [19,20] and several others [21-23]. However, a significant challenge of the classical Chan-Lam cross-coupling is with arylboronic acids bearing an electron-withdrawing substituent which is attributed to the difficulty in formation of the key ‘arylCu(III) intermediate’ [24]. The reaction is additionally guarded by the limitations of high reaction time, use of excess arylboronic acids, need for additives (molecular oxygen, pyridine-*N*-oxide, TEMPO) and possibility of a number of side reactions [25].

After the first report of a catalytic version of Chan−Lam cross-coupling by Collman, several attempts have been made by various research groups over the years to broaden the scope of Chan−Lam cross−coupling reaction [26-31]. An obvious choice of catalyst is the economically viable and easily available Cu, amidst other available transition metals like Ni, which is also reported to facilitate Chan-Lam cross-coupling [32-35].

5.2 *Heterogeneous catalysis in Chan-Lam cross-couplings*

Of several possibilities, heterogeneous adaptations of Cu are far more preferred by virtue of its easy recoverability and reusability [36-40]. In this regard, several heterogeneous catalysts have been developed to achieve efficient Chan-Lam cross-couplings. Some examples are $CoFe_2O_4$@SiO_2-NH_2-furfural-$Cu(OAc)_2$ nano magnetic catalyst [36], Cu(II)−β−cyclodextrin complex [38], MCIP [39], Cu@Fe_3O_4−TiO_2−L−dopa [40], GO@AF−SB Cu [41], *N*−enriched GO/Cu [42], Cu@PI−COF [43] etc. However, most of them faced some common challenges:

a) The catalysts are synthesized through complex multi-step procedures which may be difficult to reproduce in the laboratory;

b) Stabilizing and binding agents are required for supporting metal nanoparticles on the catalyst surface;

c) Many ligands/reagents are expensive and hard-to-find;

d) The syntheses of substrates with the help of the developed catalysts are mostly base-dependent;

e) Most catalysts are restricted to a substrate scope of Chan-Lam *N*-arylation of anilines and azoles only.

In the quest for robust and cleaner catalytic materials [44], polymeric graphitic carbon nitride (g-C_3N_4) surfaces have attracted much attention on account of its suitability in sustainable chemistry [45]. Graphitic carbon nitride (g-C_3N_4) is a polymeric material consisting mainly of C, N and a small amount of H. The atoms are linked based on heptazine (or tri-*s*-triazine) units and poly (triazine imide) units (Figure **5.1**). The most thermally (up to 600 °C in air) and chemically stable (resistant to acids, bases and organic solvents) of all carbon nitrides, g-C_3N_4 is expected to be a conjugated two-dimensional polymer of carbon, nitrogen and some hydrogen and tends to form π-conjugated planar layers held by weak van der Waals forces of attraction, similar to that in graphite [46,47]. To note, the notation "g-C_3N_4" is actually non-stoichiometric and is simultaneously used to mean both the nanosheets and the bulk material.

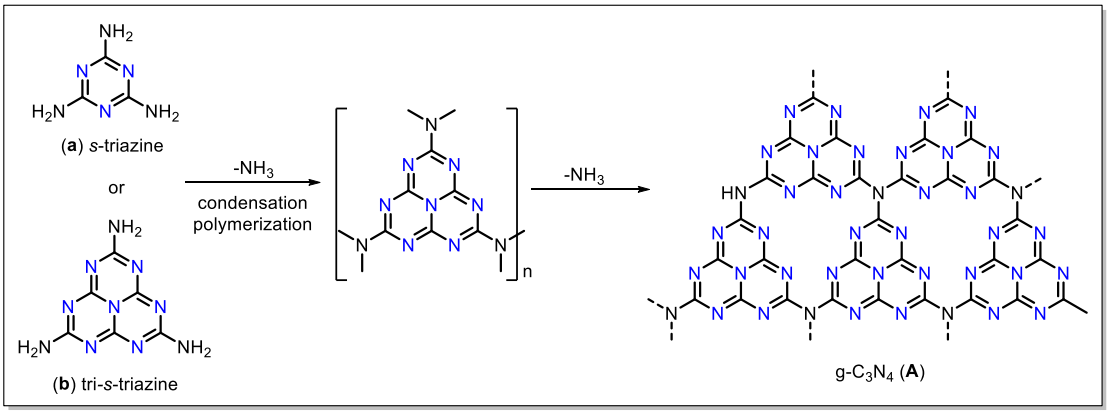

Figure **5.1** Formation of graphitic carbon nitride from *s*-triazine and tri-*s*-triazine

There have been several attempts to optimize the properties of g-C_3N_4 through functionalization of its surface with oxygen. The presence of oxygen within the polymeric matrix of g-C_3N_4 imparts Brønsted acidity in addition to the inherent Lewis basicity of the surface [48]. It also generates additional active sites and imparts a good dispersion of the material in water, which is otherwise insoluble in most organic solvents. The π-conjugated planar layers are expected to assist in anchoring the substrate. It is believed to provide sites for the dispersion of "active" metal species at the metal-surface boundary and facilitate the redox behaviour of metal NPs. The substitution of "N" by "O" in the polymer matrix is easy (Figure **5.2**).

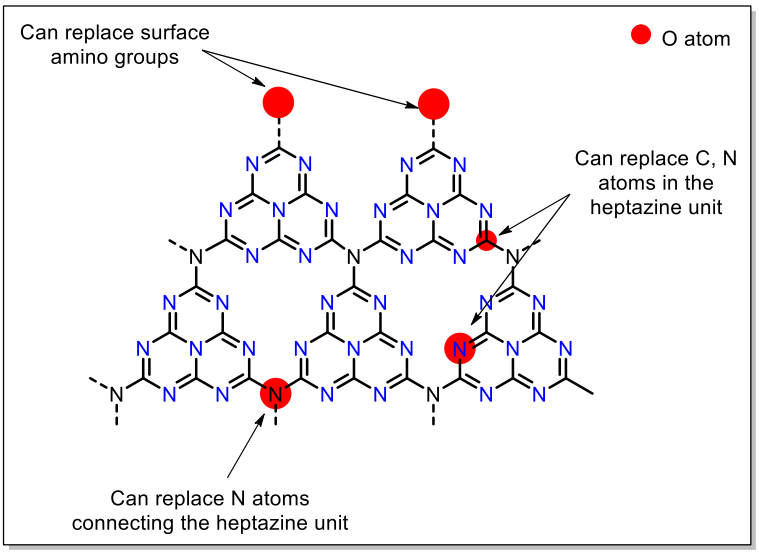

Figure **5.2** Possible replacements of oxygen atom in graphitic carbon nitride surface

Extensive studies have shown that "O" can substitute (i) the *N*-atoms "connecting" the heptazine rings or, (ii) the carbon/nitrogen atoms "forming" the heptazine rings or, (iii)

the surface amino groups, which can further transform to –OH groups and enhance the hydrophilicity of the material [49]. The catalytic potential of oxidised g-C_3N_4 has been widely explored as a photo-catalyst, in environmental remediation, hydrogen evolution, hydrogenation and singlet oxygen generation [50-54]. With the rise of extravagant catalysts for C−N bond formation reactions, we have chosen a graphitic carbon nitride oxide surface (g-C_3N_4O) and have laid emphasis on the following points for the synthesis of the catalytic material:

I. To employ non-toxic and readily available starting materials for the catalyst synthesis with the formation of minimum by-products at the end of the reaction.
II. Use of organic and non-toxic reducing agent for metal nanoparticles.
III. Use of green and biodegradable stabilizing agents for the catalysts.
IV. To promote base−free *N*−arylation whenever possible.
V. To ensure maximum recyclability and reusability of the catalyst.

5.3 *Results and Discussion*

In this chapter, we have discussed a facile synthesis of Cu(0)/g-C_3N_4O in which Cu(0) NPs were dispersed on the surface of g-C_3N_4O using an aqueous solution of L-ascorbic acid. The g-C_3N_4O surface was obtained through microwave irradiation of guanidine hydrochloride [55] and polyethylene glycol (PEG) 400, without the use of additional oxidizing agents. The as-synthesized Cu(0)/g-C_3N_4O was utilized in the Chan-Lam *N*-arylation of anilines, imidazoles/benzimidazoles and Indoles with arylboronic acids. The catalyst could be credited for a simple preparation route involving microwave irradiation [56] and participation of the *N*-rich sites as Lewis bases in achieving the desired transformation.

5.3.1 *Characterization of the Catalyst*

Due to the presence of excess oxygen on the surface, g-C_3N_4O is water-soluble and its spectral properties vary significantly from g-C_3N_4, as is evident from the following discussion. The graphitic sheet is not formed in the absence of PEG, which suggests that PEG plays an important role in formation of the oxygenated sheet. On account of such properties, the surface of g-C_3N_4O is chosen as a heterogeneous support for Cu(0) NPs.

The bulk morphology of Cu(0)/g-C_3N_4O is studied by high resolution transmission electron microscope (HRTEM) (Figure **5.3**). The TEM images suggest decoration of spherical Cu(0) NPs on the surface of g-C_3N_4O (Figure **5.3a**). HRTEM image of Cu(0) NPs shows the presence of lattice fringes with an interlayer spacing of 0.205 nm (Figure **5.3b**). The Selected Area Electron Diffraction (SAED) pattern analysis of Cu(0)/g-C_3N_4O indicates the crystalline nature of Cu(0) NPs (Figure **5.3c**). The lattice planes (111), (200) and (220) obtained in the SAED pattern belong to the crystal lattice of Cu(0) NPs which correlates with the powder X-ray diffraction (p-XRD) pattern (Figure **5.4b**). The particle size distribution histogram shows Cu(0) NPs in an average size range of 7-8 nm (Figure **5.3d**). The p-XRD patterns of g-C_3N_4O and Cu(0)/g-C_3N_4O indicates significant changes in the graphitic structure after immobilization of the Cu(0) NPs on the g-C_3N_4O surface (Figure **5.4**).

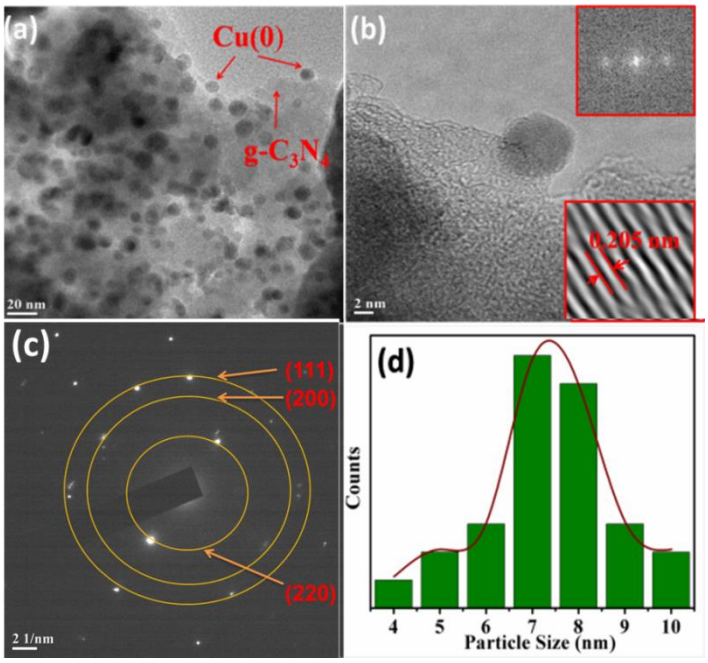

Figure **5.3** TEM images of: (**a**) Cu(0) NPs decorated on g-C_3N_4O surface; (**b**) HRTEM image of Cu(0)/g-C_3N_4O (inset shows the lattice fringes); (**c**) SAED pattern for Cu(0)/g-C_3N_4O; (**d**) Particle size distribution curve of Cu(0)/g-C_3N_4O

The graphitic stacking pattern in oxidized carbon nitride is commonly characterized by two values of the *d*(002) plane [57]. In addition to a broadened (002) graphitic peak at 2θ = 27.2° (*d* = 0.329 nm), the strong diffraction peak at 2θ = 32.7° (*d* = 0.273 nm) denotes a reduction in the interplanar distance between the melem planes on oxidation

[58] (Figure **5.4a**). A diminished (100) peak indicates the replacement of some carbon atoms in the heptazine ring with oxygen in g-C_3N_4O [59]. The diffraction peak at 2θ = 23.1° (*d* = 0.384 nm) is attributed to PEG [60]. The p-XRD pattern of Cu(0)/g-C_3N_4O (Figure **5.4b**) gives prominent indication of the formation of Cu(0) with sharp diffraction peaks at 2θ = 43.4° (*d* = 0.208 nm), 2θ = 50.6° (*d* = 0.180 nm) and 2θ = 74.2° (*d* = 0.127 nm) indexed as (111), (200) and (220) crystal planes of metallic Cu(0) respectively (JCPDS Card No-85-1326). A high loading and high crystallinity of Cu(0) NPs diminish the intensity of graphitic surface peaks in the p-XRD pattern of the synthesized Cu(0)/g-C_3N_4O [61]. A comparative FT−IR analysis of g-C_3N_4O and Cu(0)/g-C_3N_4O (Figure **5.5a**) shows changes in the intensities of bare g-C_3N_4O after immobilization of the Cu(0) NPs.

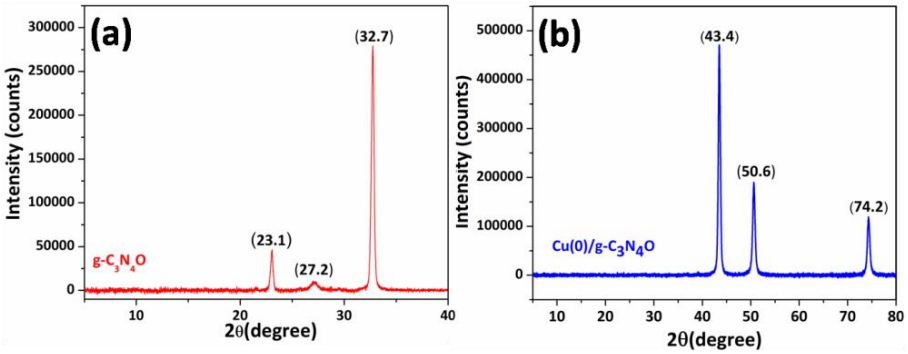

Figure **5.4** p-XRD pattern of (**a**) bulk g-C_3N_4O; (**b**) Cu(0)/g-C_3N_4O

The sharp absorption bands at around 3000-3100 cm^{-1} can be assigned to the N-H stretching modes while the stretching vibrations at 1647, 1408 and 1080 cm^{-1} can be assigned to both the aromatic C=N and C=O heterocyclic motifs, N-O and C-O bonds, respectively. The breathing mode of heptazine unit at 807 cm^{-1} confirms the presence of the tri-*s*-triazine unit in both g-C_3N_4O and Cu(0)/g-C_3N_4O [48,59]. UV−Vis spectral analysis (Figure **5.5b**) of Cu(0)/g-C_3N_4O also reveals changes in the characteristic absorption bands of g-C_3N_4O which indicates the blue shift of $\pi \rightarrow \pi^*$ transition from 220 nm to deep UV region and $n \rightarrow \pi^*$ transition from 332 nm to 254 nm. Further evidence of the formation of Cu(0)/g-C_3N_4O is the broad and continuous SPR peak of Cu(0) around 550 nm which transcends to near-IR region [62]. EDX spectrum of Cu(0)/g-C_3N_4O confirms the presence of Cu (Figure **5.5c**). Peaks for Cu are observed at 0.9297 keV ($Cu_{L\alpha 1,2}$), 8.0478 keV ($Cu_{K\alpha 1,2}$) and 8.9052 keV ($Cu_{K\beta 1}$) respectively [63]. ICP-AES analysis of Cu(0)/g-C_3N_4O reveals 6.02 wt% of Cu(0) deposition on the g-C_3N_4O surface.

The surface area and porosity of the synthesized Cu(0)/g-C_3N_4O are measured by N_2 adsorption-desorption analysis at 77 K. The N_2 adsorption-desorption isotherm (Figure **5.5d**) corresponds to a Type-IV isotherm, typical of porous materials with a H4 hysteresis loop. According to BET analysis, the surface area (S_{BET}) of g-C_3N_4O and that of the synthesized Cu(0)/g-C_3N_4O are found to be 39.293 m^2/g and 21.823 m^2/g respectively, which is larger than that of traditional bulk g-C_3N_4 [64-65].

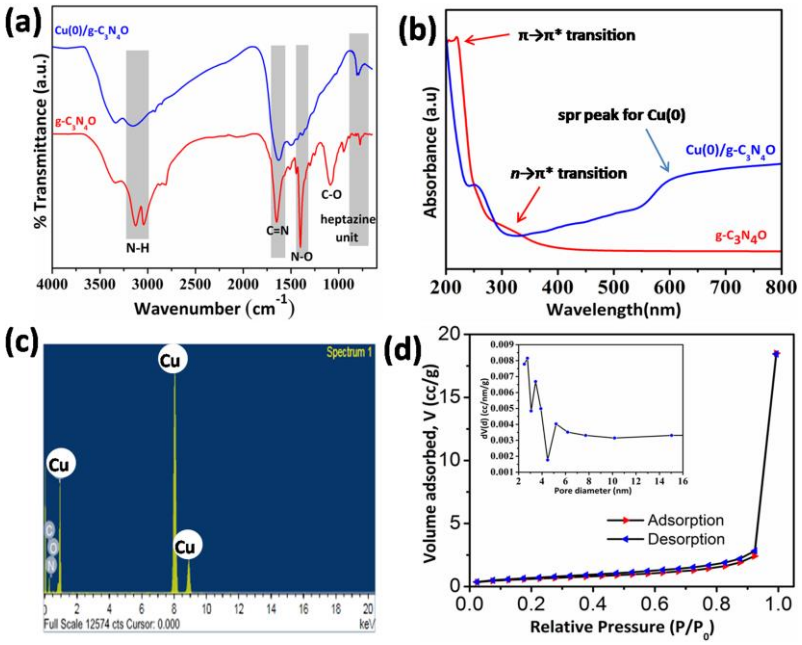

Figure **5.5** (**a**) FT-IR spectra of [red: bulk g-C_3N_4O; blue: Cu(0)/g-C_3N_4O]; (**b**) UV–Vis absorption spectra of [red: bulk g-C_3N_4O; blue: Cu(0)/g-C_3N_4O] in EtOH; (**c**) EDX plot of Cu(0)/g-C_3N_4O; (**d**) N_2 adsorption-desorption isotherm of Cu(0)/g-C_3N_4O at 77 K (inset shows the pore size distribution curve of Cu(0)/g-C_3N_4O).

The pore size distribution calculated from desorption loop of the isotherm by the BJH method, indicates the mesoporous nature of Cu(0)/g-C_3N_4O with a pore volume of 0.286 cc/g and pore radius of 1.37 nm, respectively [66-67].

The elemental composition and their state in Cu(0)/g-C_3N_4O is investigated by XPS. The full scan survey XPS spectrum of Cu(0)/g-C_3N_4O is shown in Figure **5.6a**. The sharp binding energy peaks at 285, 399, 531 and 932.5 eV corresponds to the C, N, O and Cu elements of Cu(0)/g-C_3N_4O respectively. The deconvoluted Cu 2p XPS spectrum depicts peaks with binding energies at 932.2 and 951.9 eV that belong to the Cu $2p_{3/2}$ core level and Cu $2p_{½}$ core level spin-orbit splitting respectively (Figure **5.6b**). These are suggestive

of the presence of Cu(0) on the surface of g-C_3N_4O. Subsequently, the C 1s XPS spectrum shows four peaks with binding energies at 284.8, 287, 287.9 and 289.2 eV (Figure **5.6c**). The peaks are assigned to C-C/C=C, C-N/C=N, C=O and O=C-OH bonds respectively. The bonds attributed to C=C and C=N are that of the sp^2 carbon atom in the *s*-triazine ring. The high-resolution N 1s spectrum is deconvoluted to three distinct peaks at 399.2, 400.7 and 401.6 eV.

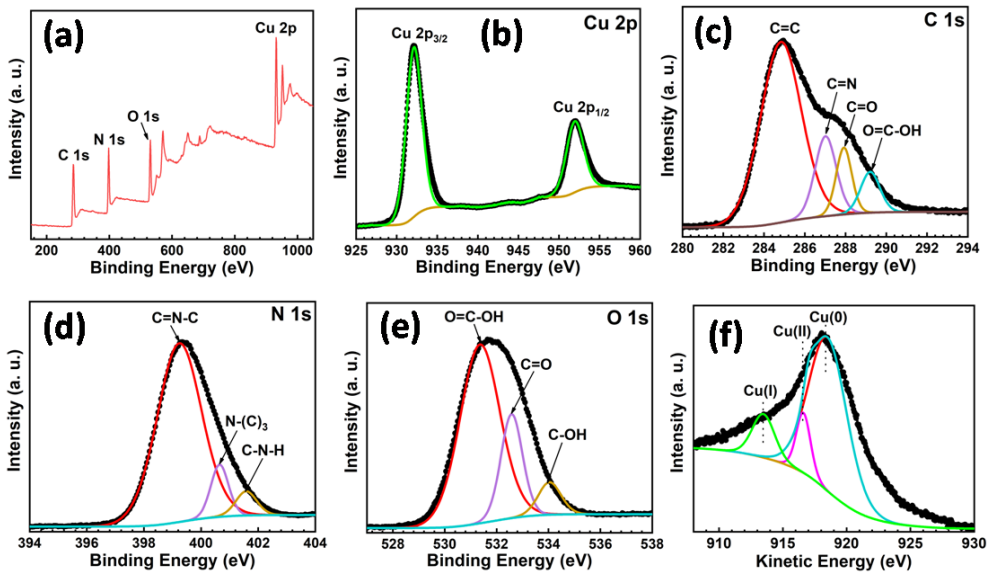

Figure **5.6** (**a**) Full scan survey XPS spectrum of Cu(0)/g-C_3N_4O and the corresponding high-resolution deconvoluted XPS spectra of (**b**) Cu 2p; (**c**) C 1s; (**d**) N 1s; (**e**) O 1s and (**f**) deconvoluted Cu LMM Auger spectrum of Cu(0)/g-C_3N_4O

These are attributed to pyridine-like sp^2 (C=N−C) nitrogen of the triazine ring, the nitrogen atom which is trigonally bonded to the carbon atom in the C-N network (N−(C_3)) and the C−N−H bond, respectively (Figure **5.6d**) [68]. The high-resolution O 1s spectrum is fitted with three binding energy peaks at 531.4, 532.6 and 404 eV attributed to the O=C−OH, C=O and C−O groups respectively (Figure **5.6e**) [48]. Figure **5.6f** shows the deconvoluted Auger Cu 2p LMM spectrum of Cu(0)/g-C_3N_4O. The fitting of Cu LMM Auger spectrum is performed by three peaks with kinetic energies of 914, 917.1 and 918.5 eV, corresponding to Cu(I), Cu(II) and Cu(0) species respectively. The sharp kinetic energy peak obtained at 918.5 eV confirms the formation of Cu(0) on the g-C_3N_4O surface [69]. The low intensity peaks obtained for Cu(I) and Cu(II) at the

deconvoluted Cu LMM Auger spectrum are due to the partial oxidation of Cu(0) during the XPS sample preparation.

Inspired by the stability and sustainability of Cu(0)/g-C_3N_4O, we employed it in the Chan-Lam cross-coupling of phenylboronic acids with anilines (Table **5.2**), 1*H*−imidazoles and 1*H*−benzimidazoles (Table **5.4**) and Indoles (Table **5.6**).

5.3.2 *Optimization of reaction conditions*

For the initial screening of reaction conditions, 4−Methoxyphenylboronic acid (**1a**) and aniline (**2b**) were taken as model substrates (Table **5.1**). At first, they were reacted with 1 wt% (0.075 mol% of Cu) of Cu(0)/g-C_3N_4O and K_2CO_3 in water at room temperature and open air condition (Table **5.1**, entry **1**). Phenylboronic acid was completely consumed in 6 h and two products were obtained. The expected Chan−Lam product was obtained in 78% yield and the collateral C−C coupling product in 20% yield. To improve the obtained yield of the *N*-arylated product and minimize the homocoupling of phenylboronic acids, the reaction was monitored by altering the reaction conditions. Increasing the amount of catalyst to 2 wt% (0.14 mol% of Cu) did give us better results (Table **5.1**, entry **2**), but further increase to 3 wt% (0.208 mol% of Cu) and 5 wt% (0.35 mol% of Cu) gave us similar yields of the same product (Table **5.1**, entries **3** and **4**). Protic solvents like isopropanol and methanol and aprotic solvents like acetonitrile and DMSO were screened for the arylation reaction (Table **5.1**, entries **5-8**). The progress of the reaction was either similar or slightly better than that in water. It did not proceed in toluene (Table **5.1**, entry **9**). Inorganic bases like K_2CO_3, NaOH, KO^{t}Bu and organic bases like DABCO, and Et_3N gave similar yields of the desired product (Table **5.1**, entries **10-13**). Encouraged by the presence of basic surface sites on g-C_3N_4O, we also tested the reaction in base-free conditions. Unexpectedly, the catalyst showed better activity in the absence of a base (Table **5.1**, entry **15**). Also, the formation of the C−C coupling product was greatly diminished. The absence of an external base probably limits the coupling of phenylboronic acids in the presence of Cu [70]. An increase in temperature, however, could not increase the yield of the *N*−aryl product further (Table **5.1**, entries **16** and **17**).

Table **5.1** Investigation of reaction conditions for the Chan-Lam *N*–arylation of aniline (**2b**) with 4–Methoxyphenylboronic acid (**1a**).[a]

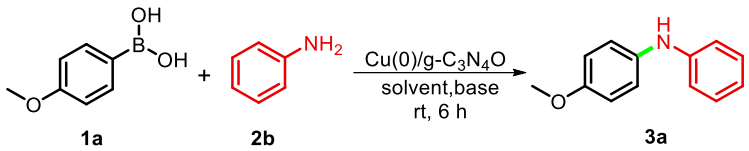

1a **2b** **3a**

Entry	Cu(0)/g-C_3N_4O (wt%)	Base	Solvent	Yield[b] (%)
1	1	K_2CO_3	Water	78
2	2	K_2CO_3	Water	80
3	3	K_2CO_3	Water	75
4	5	K_2CO_3	Water	75
5	2	K_2CO_3	isopropanol	75
6	2	K_2CO_3	Methanol	82
7	2	K_2CO_3	CH_3CN	64
8	2	K_2CO_3	DMSO	75
9	2	K_2CO_3	Toluene	NR
10	2	DABCO	Water	56
11	2	NaOH	Water	55
12	2	KO^{t}Bu	Water	55
13	2	Et_3N	Water	50
14	2	-	Methanol	85
15	**2**	**-**	**Water**	**93**
16[c]	2	-	Water	90
17[d]	2	-	Water	87

[a]*Reaction conditions*: 4-Methoxyphenyl boronic acid, **1a** (1 mmol), Aniline, **2b** (0.8 mmol), solvent (4 mL), room temperature, 6 h; [b]Isolated yield based on Aniline, **2b** [c], [d]Reaction temperature was maintained at 40 °C and 60 °C respectively; NR- no reaction

5.3.3 *Substrate scope study*

The optimized reaction conditions were employed in the study of Chan-Lam *N*-arylation of anilines. Table **5.2** reflects the wide substrate scope of our methodology. Various *o*–, *m*– and *p*–substituted arylboronic acids (**1**) have reacted with differently substituted anilines (**2**) under the optimized reaction condition (Table **5.1**, entry **15**) to give the respective *N*-aryl product (**3a-n**) in moderate to good yields (**55-93%**). The unsubstituted *N*-arylaniline (**3b**) was obtained in a good yield of 81%. Electron donating

groups (EDGs) like 4–OMe (**3a**, **3i**, **3k**, **3l**), 4–Et (**3c**) on the phenylboronic acid had shown a higher reaction rate in comparison to those with electron withdrawing groups (EWGs) like 3–CF_3 (**3e**). But the reaction did not proceed with phenylboronic acids bearing strongly withdrawing groups like –NO_2 and –CN [31]. Substrates like Naphthalene-2-boronic acid (**3d**) and 2-Methoxypyridine-5-boronic acid (**3f**) were also tolerated. In case of anilines, the protocol not only endured anilines with EDGs (**3i**, **3j**) and EWGs (**3n**), but their scope also extended to sterically hindered 2,4-Dimethylaniline (**3k**), benzylamine (**3l**) and that bearing electron withdrawing –NO_2 group (**3n**) in 55%, 72% and 65% yields respectively. Anilines with weakly deactivating –Br group (**3g**, **3h**) also gave the corresponding *N*-arylated product in good yields.

Table **5.2** Scope exploration of the Chan-Lam *N*-arylation of anilines (**2**) with phenylboronic acids (**1**).[a]

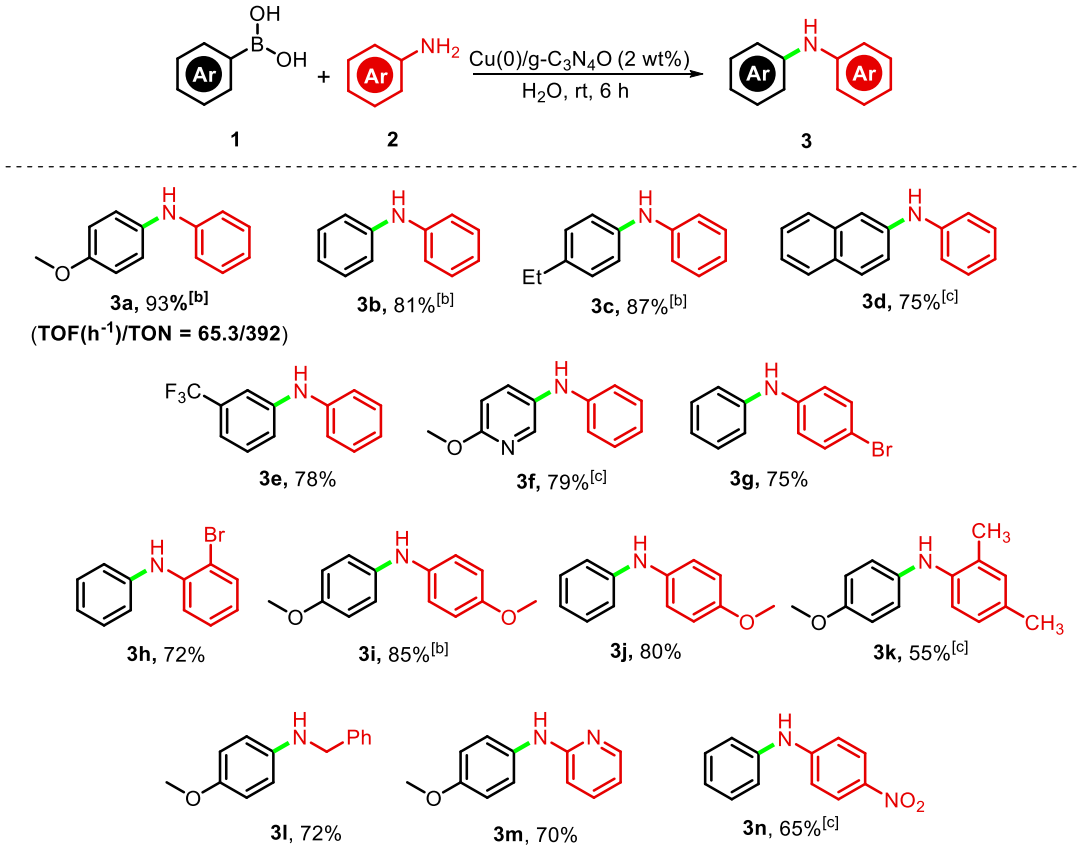

[a]*Reaction conditions*: Arylboronic acid, **1** (1 mmol), aniline, **2** (0.8 mmol), Cu(0)/g-C_3N_4O (2 wt%), H_2O (4 mL), room temperature, 6 h; Isolated yield based on **2**; [b]C–C coupling product observed in addition to the *N*-aryl product; [c]reaction time extended to 10 hours.

5.3.4 *Mechanism Study*

The involvement of a Cu(0) NPs in our protocol may slightly differ the proposed mechanistic route from the classical approach. A series of controlled reactions was carried out to confirm the involvement of "Cu(0)/g-C_3N_4O system" in the formation of *N*-aryl products (Scheme **5.1**). It was observed that the reaction did not proceed with the bare support (g-C_3N_4O) indicating the inefficiency of bulk g-C_3N_4O alone, while it proceeded faintly (35% of **3a**) in the presence of $CuCl_2$. The combination of $CuCl_2$+g-C_3N_4O also produced a low product yield, which proved the efficiency of Cu(0) supported g-C_3N_4O in the reaction medium.

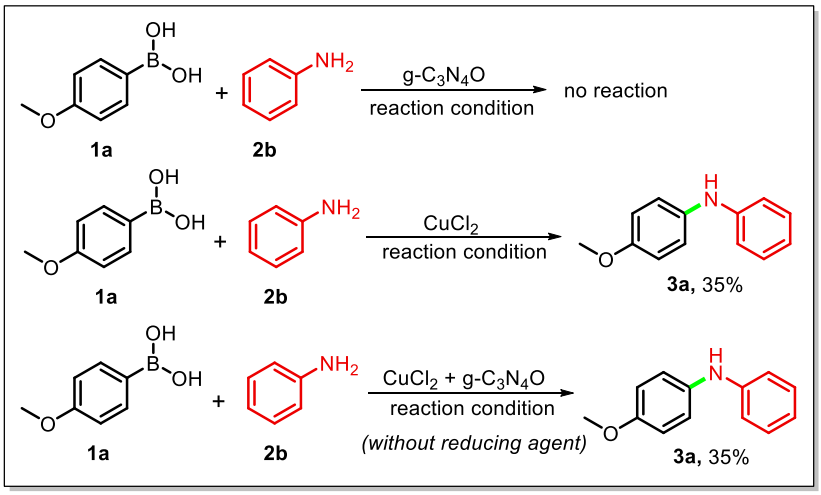

Scheme **5.1** Study of controlled reactions

5.3.5 *Plausible Mechanism*

Based on the above observations, the plausible mechanism is shown in Figure **5.7**. The Cu(0) nanoparticles (NPs) stabilized on the surface of g-C_3N_4O acts as a pre-catalyst and undergoes "gradual" oxidation to Cu(II) [71]. During the reaction, Cu(0) NPs are slowly oxidized to Cu(II) which facilitates the Chan-Lam cross-coupling reaction through the regular reaction pathway involving transmetallation and disproportionation. The basicity of the nitrogen atoms on the surface of g-C_3N_4O facilitates deprotonation of the amine [48,72]. The aryl group of the phenylboronic acid then adds to the Cu(II) centre on the surface of g-C_3N_4O at the stage of transmetallation [73]. Here, water plays a crucial role in generating the tetrahedral $[ArB(OH)_3]^-$ anion on interaction with phenylboronic acid [74-75]. The Cu(II) species then undergoes the rate-determining

disproportionation step to the Cu(III) intermediate, leading to facile reductive elimination of the product (**3**) [76]. After reductive elimination of the product, the resulting Cu(I) are re-oxidized to Cu(II) on the surface of g-C_3N_4O and the catalytic cycle goes on. The stabilization of Cu(0) NPs on the surface of g-C_3N_4O is a crucial factor for the reaction. The oxidation of Cu(0) to Cu(II) must take place in a "controlled" manner. That is why, when most of the Cu(0) NPs are oxidized to Cu(II) after the fifth run of the catalyst, the reaction yield significantly decreases to 85%.

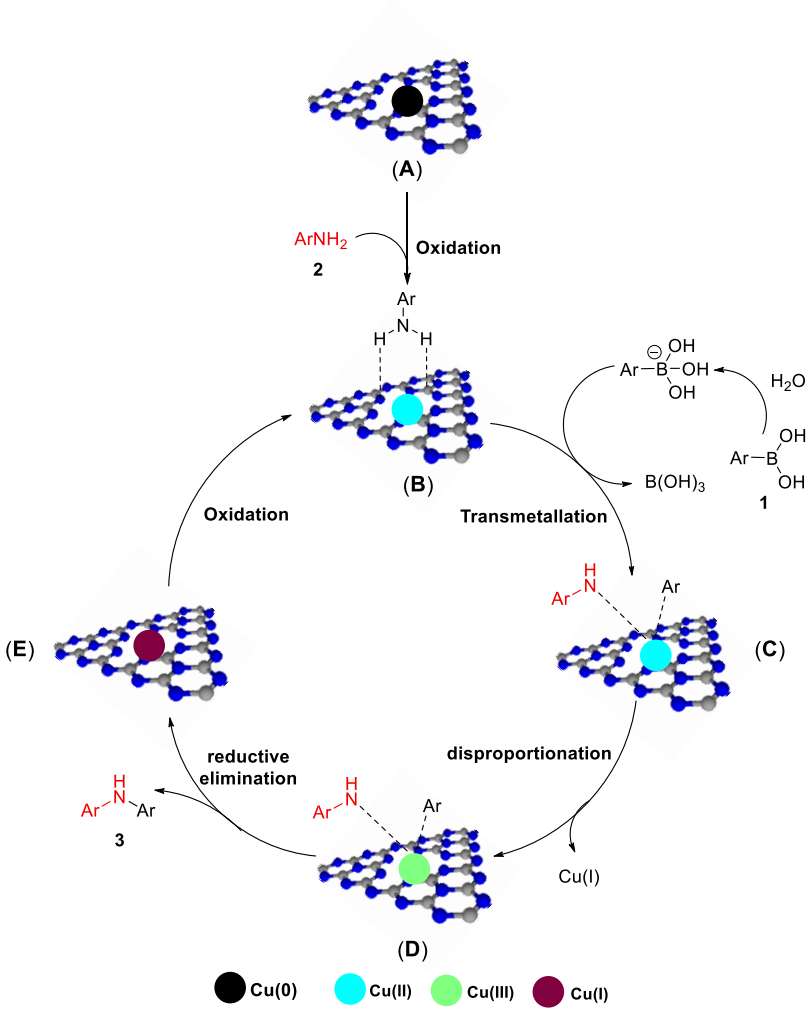

Figure **5.7** Plausible Mechanism

The catalyst was tested for heterogeneity (Refer section 5.3.8.4 for details) and was successfully reused up to the fifth cycle (Figure **5.8**) without significant loss of catalytic activity. The TON and TOF of the catalyst was found to be 392 and 65.3 h^{-1} respectively [77-79].

Kinetic study of the catalyst (GC analysis) was performed under the optimized reaction condition (Table **5.1**, entry **15**). It shows that the catalyst was fairly stable up to five runs of the reaction (Figure **5.9**). Gradual deactivation may occur due to oxidation of Cu or subsequent loss of active sites. Further, XPS studies were carried out for the reused catalyst after the fifth run to study the oxidation state of Cu after reuse. Figure **5.10a** shows the high resolution deconvoluted XPS spectrum of Cu 2p. The high-resolution Cu 2p spectrum fitted with four different peaks corresponds to the spin-orbit splitting of Cu $2p_{3/2}$ and Cu $2p_{1/2}$ respectively. The peaks obtained at binding energies of 932.1 and 951.9 eV belongs to Cu(0) and that at 933.5 and 953.5 eV belongs to Cu(II). Besides, two "shakeup" satellite peaks at around 942 eV and 961.1 eV indicated the presence of Cu(II) ions due to partial oxidation of Cu(0) to Cu(II) in Cu(0)/g-C_3N_4O during the Chan-Lam *N*-arylation reaction. The high-resolution deconvoluted O 1s spectrum was obtained with three binding energy peaks at 531.4 eV, 532.5 eV and 534 eV corresponding to O=C−OH, C=O and C−OH groups, respectively (Figure **5.10b**). The increase in intensity of the peak attributed to C−OH group in the recycled catalyst also confirmed the partial oxidation of Cu(0) after the fifth run. Figure **5.10c** shows the deconvoluted Auger Cu 2p LMM spectrum of the reused catalyst after the fifth run. The fitting of Cu LMM Auger spectrum was performed by three peaks similar to the fresh catalyst, corresponding to Cu(I), Cu(II) and Cu(0) species, respectively. The sharp kinetic energy peak obtained at 917.1 eV confirmed the oxidation of Cu(0) to Cu(II) on the g-C_3N_4O surface after the fifth run.

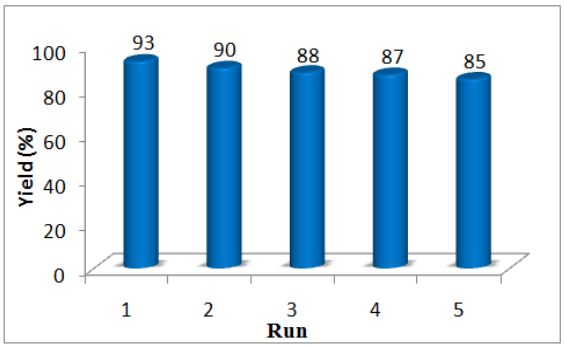

Figure **5.8** Recyclability of Cu(0)/g-C_3N_4O

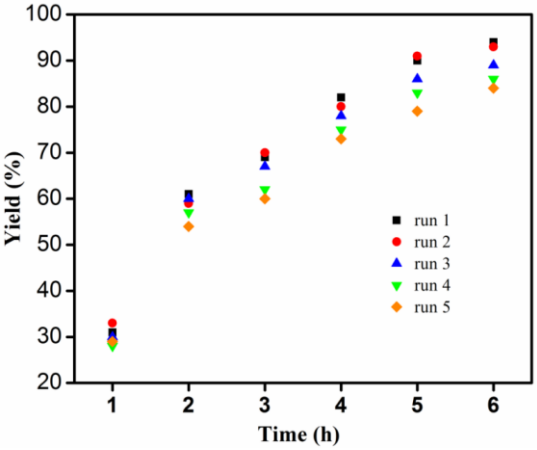

Figure **5.9** Study of stability (time-resolved) of the catalyst Cu(0)/g-C_3N_4O.

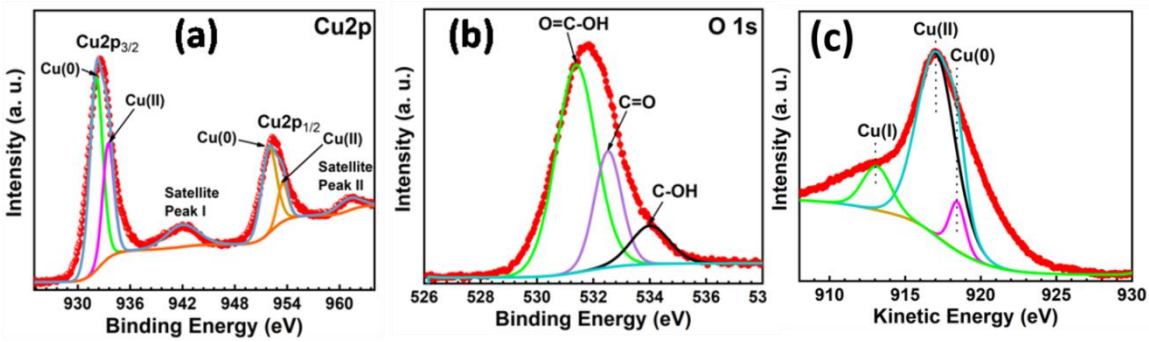

Figure **5.10** High-resolution deconvoluted XPS spectra of (**a**) Cu 2p and (**b**) O 1s of recycled Cu(0)/g-C_3N_4O catalyst; and (**c**) deconvoluted Cu LMM Auger spectrum of recycled Cu(0)/g-C_3N_4O catalyst after the fifth run.

5.3.6 *Extension of scope of reaction*

With encouraging results in hand, the scope of Cu(0)/g-C_3N_4O was extended to the Chan-Lam cross-coupling of phenylboronic acids with 1*H*-imidazoles and 1*H*-benzimidazoles. Various reaction conditions were examined and the results are listed in Table **5.3**. With 4−Methoxyphenylboronic acid (**1a**) and 4(5)−Methyl-1*H*-imidazole (**4a**) as the model substrates, the highest yield was obtained under a base-free condition in methanol (Table **5.3**, entry **6**). Inspired by the ability of imidazoles to also act as bases [80-81], our initial investigation began in a base-free condition. Different polar and non-polar solvents were screened under base-free conditions (Table **5.3**, entries **1-5**). It was seen that the reaction proceeded fairly in polar protic solvents like methanol and polar aprotic solvents like acetonitrile and DMSO. But, it did not show any results in water

and toluene, probably due to their low solubility in these solvents. Similar to anilines, only 2 wt% (0.15 mol% of Cu) of the catalyst was sufficient to catalyze the cross-coupling of the model substrates at 'open-flask' room temperature condition in methanol (Table **5.3**, entries **6** and **7**). The reaction was also tested in the presence of a number of bases (Table **5.3**, entries **8-11**). The addition of inorganic bases like K_2CO_3, NaOH and organic bases like DABCO and Et_3N produced yields which were similar to that obtained without base (Table **5.3**, entries **1-7**). A rise in temperature did not affect the yield of the *N*-aryl product (Table **5.3**, entries **12** and **13**).

Table **5.3** Investigation of reaction conditions for the Chan-Lam *N*-arylation of 4(5)-Methyl-1*H*-imidazoles (**4a**) with 4-Methoxyphenylboronic acid (**1a**).[a]

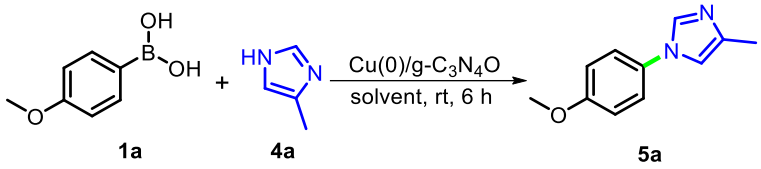

1a **4a** **5a**

Entry	Cu(0)/g-C_3N_4O (wt%)	Base	Solvent	Yield[b] (%)
1	1	-	Water	No reaction
2	1	-	Methanol	83
3	1	-	CH_3CN	68
4	1	-	DMSO	73
5	1	-	Toluene	NR
6	**2**	**-**	**Methanol**	**91**
7	3	-	Methanol	90
8	2	K_2CO_3	Methanol	85
9	2	DABCO	Methanol	82
10	2	NaOH	Methanol	75
11	2	Et_3N	Methanol	87
12[c]	2	-	Methanol	90
13[d]	2	-	Methanol	85

[a]*Reaction conditions*: 4-Methoxyphenylboronic acid, **1a** (1 mmol), 4(5)-Methyl-1*H*-imidazole, **4a** (0.8 mmol), solvent (4 mL), room temperature, 6 h; [b]Isolated yield based on **4a;** [c],[d]Reaction temperature was maintained at 40 °C and 60 °C respectively

With the optimized reaction conditions, the substrate scope of *N*-arylation of 1*H*–imidazoles and 1*H*–benzimidazoles are presented in Table **5.4**. As shown, a decent range of *N*-aryl-1*H*-imidazoles and *N*-aryl-1*H*-benzimidazoles (**5a-l**) were obtained in moderate to good yields (**70-91%**). It was seen that phenylboronic acid with an EDG such as 4–OMe, 3–Me, 2–Me (**5a**, **5b**, **5g**, **5i**) produced greater yields of the *N*-arylated product than with EWGs like 3–NO_2 and 3–CN (**5h** and **5j**). The presence of weakly deactivating –F group on the phenylboronic acid (**5f**) had also successfully given the *N*-arylated product in 88% yield. The absence of electronic effect decreased the yield of the unsubstituted product to 70% (**5c**). On the other hand, 1*H*–imidazoles with only EDGs were tested under this protocol. 1*H*–benzimidazole and 2-amino-1*H*–benzimidazole were also *N*-arylated (**5k** and **5l**) under the optimized reaction condition with 75% and 78% yield respectively. In case of 2-Amino–1*H*–benzimidazole, the N^1–arylated product was produced exclusively (**5l**).

Table **5.4** Scope exploration of the Chan-Lam *N*-arylation of 1*H*-imidazoles and 1*H*-benzimidazoles (**4**) with phenylboronic acids (**1**).[a]

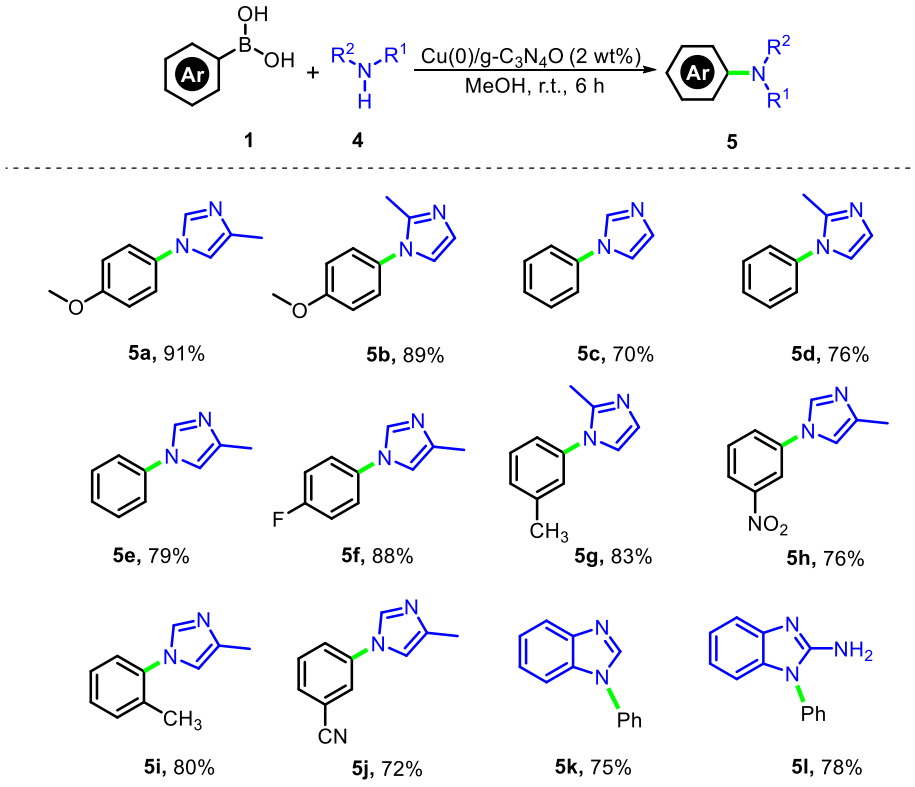

[a]*Reaction conditions*: Arylboronic acid, **1** (1 mmol), Azole, **4** (0.8 mmol), Cu(0)/g-C_3N_4O (2 wt%), MeOH (4 mL), room temperature, 6 h; Isolated yield based on **4**.

Surprisingly, when 2-amino-1*H*-benzimidazole was tested with the optimized reaction condition of anilines (Table **5.1**, entry **15**), *N*-diaryl-2-Amino-1*H*-benzimidazole (**5m**) was obtained as the major product (Scheme **5.2**). Such di-aryl-C-amino-*NH*-azoles have widespread occurrence in pharmaceuticals, agro-chemicals and biologically active scaffolds [36].

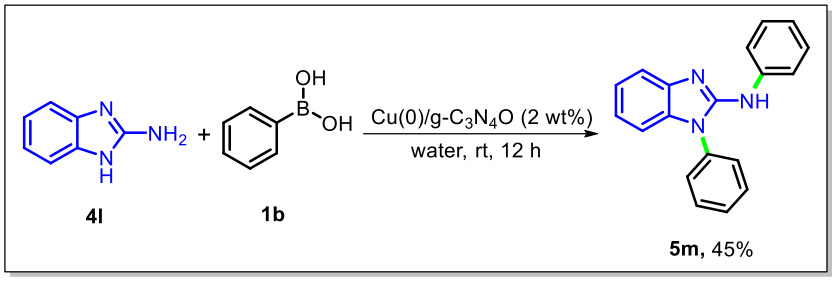

Scheme **5.2** *N,N'*-diarylation of 2-Aminobenzimidazole

To further expand the horizon of Cu(0)/g-C_3N_4O, it was also tested in the *N*-arylation of Indoles with phenylboronic acids as the arylating source. Pharmaceutically significant *N*-arylindoles can act as angiotensin II-1 antagonists, antipsychotic agents and serve as intermediates for the synthesis of other biologically active scaffolds [82]. The reaction conditions for the synthesis of *N*-arylindoles were optimized and the results are shown in Table **5.5**. The model substrates, phenylboronic acid (**1b**) and indole (**6a**) were subjected to different polar/non-polar solvents (Table **5.5**, entries **1-5**), different catalyst loadings (Table **5.5**, entries **6-8**) and different organic/inorganic bases (Table **5.5**, entries **10-14**). Polar solvents, other than water, raised the yield of *N*-arylation, while non-polar solvents like toluene could not afford the desired product (Table **5.5**, entry **1-5**). Among the screened solvents, DMSO gave the highest yield of 40% (Table **5.5**, entry **4**). To the best of our knowledge, DMSO plays a role in increasing the acidity of the N-H proton through its strong H−bond accepting ability [83]. The arylation reaction was first screened with 1 wt% of the catalyst, Cu(0)/g-C_3N_4O. Thereafter, the effect of increase in catalyst loading on the arylation reaction was monitored. It was seen that 3 wt% of the catalyst gave highest yield of the arylated product (Table **5.5**, entries **6-8**). While, temperature played a crucial role in raising the yield of *N*-arylindole (Table **5.5**, entries **9** and **10**), K_2CO_3 proved to be most effective among different bases like NaOH, DABCO, KO^{t}Bu and Et_3N for the arylation reaction (Table **5.5**, entries **10-14**). Unlike previous *N*-nucleophiles, only 35% of the desired product was obtained under

base-free reaction conditions, probably due to lower acidity of the indole N−H proton (pK_a = 16.97) [84]. Subjected to all the above, the optimized reaction condition was fixed at 80 °C with 3 wt% (0.33 mol% of Cu) of Cu(0)/g-C_3N_4O in DMSO (Table **5.5**, entry **10**).

Table **5.5** Investigation of reaction conditions for the Chan-Lam *N*-arylation of Indole (**6a**) with phenylboronic acid (**1b**).[a]

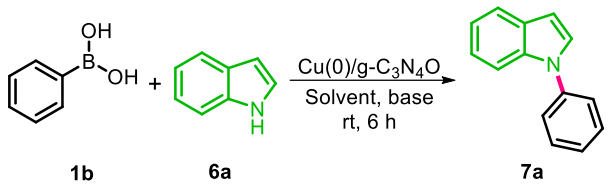

1b **6a** **7a**

Entry	Cu(0)/g-C_3N_4O (wt%)	Base	Solvent	Yield[b] (%)
1	1	K_2CO_3	Water	NR
2	1	K_2CO_3	Methanol	30
3	1	K_2CO_3	ACN	33
4	1	K_2CO_3	DMSO	40
5	1	K_2CO_3	Toluene	NR
6	2	K_2CO_3	DMSO	42
7	3	K_2CO_3	DMSO	45
8	5	K_2CO_3	DMSO	48
9[c]	3	K_2CO_3	DMSO	75
10[d]	**3**	**K_2CO_3**	**DMSO**	**87**
11[d]	3	DABCO	DMSO	80
12[d]	3	NaOH	DMSO	77
13[d]	3	KO^{t}Bu	DMSO	75
14[d]	3	Et_3N	DMSO	80
15[d]	3	-	DMSO	35

[a]*Reaction conditions*: Phenylboronic acid, **1b** (1 mmol), Indole, **6a** (0.8 mmol), base (1 equiv.), solvent (4 mL), 80 °C, 6 h; [b]Isolated yield based on **6a** [c], [d]Reaction temperature was maintained at 60 °C and 80 °C respectively.

The best reaction condition was utilized to generate a wide substrate scope of *N*-arylindoles (Table **5.6**). Variously substituted *N*-aryl indoles (**7a**-**i**) were obtained in

moderate to good yields (**60-87%**). As evident from Table **5.6**, when unsubstituted phenylboronic acid was reacted with indole, 87% of the *N*-arylated product (**7a**) was obtained. Phenylboronic acids with EDGs like 3−Me, 4−OMe and 4−Et gave very good yields of *N*-arylindoles (**7f**, **7i**). However, when phenylboronic acids with EWGs like 3−CF_3 and 4−CN were employed for arylation, the yields of the subsequent *N*-arylindoles were significantly lowered (**7g**, **7h**). Similarly, indoles with EDGs (**7c**, **7d**) reacted smoothly in comparison to those with EWGs (**7b**). To our surprise, Indole nucleus with a weakly deactivating –Br group at the 7th position (**7e**) was also arylated exclusively. All the observations were in agreement with the effect of electronic factors in the Chan-Lam cross-coupling of *N*-nucleophiles. Owing to the pharmaceutical significance of *N*-arylindoles, the above methodology was applied on a 10 mmol scale. The desired *N*-arylated indole was generated in 83% yield (Table **5.6**). This scale-up attempt depicted the efficacy of the catalyst on a gram scale.

Table **5.6** Scope exploration of the Chan-Lam *N*-arylation of Indoles (**6**) with phenylboronic acids (**1**).[a]

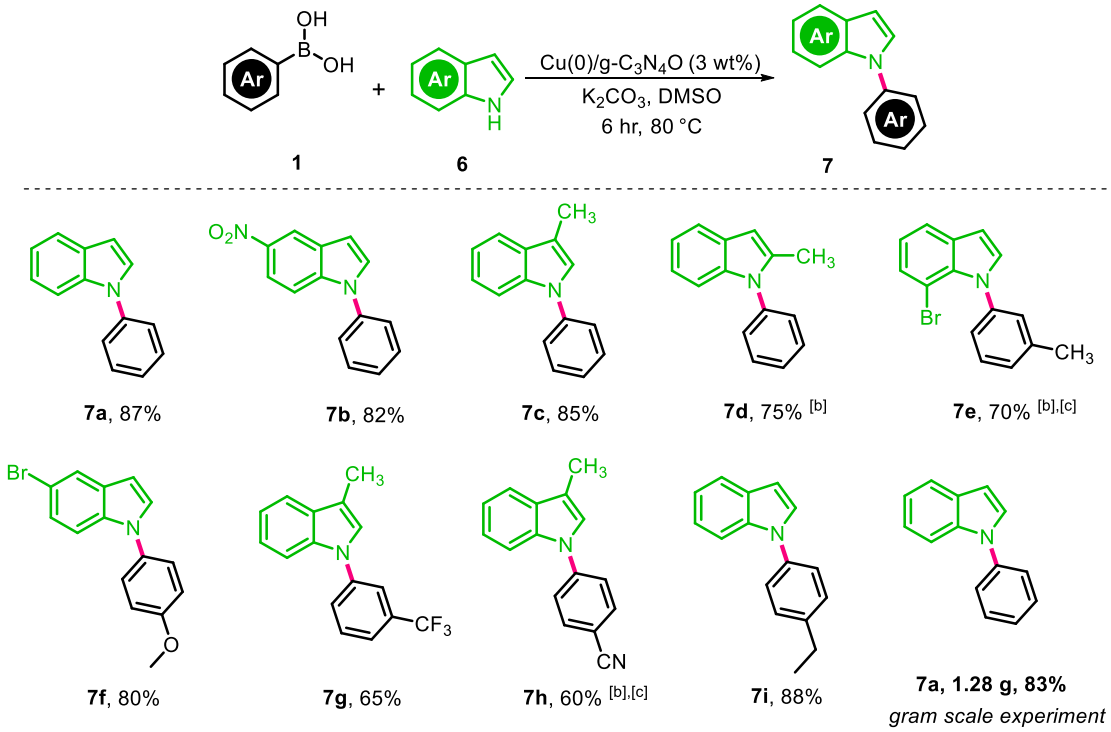

[a]*Reaction conditions*: arylboronic acid **1** (1 mmol), **6** (0.8 mmol), Cu(0)/g-C_3N_4O (3 wt%), K_2CO_3 (1 equiv.), DMSO (4 mL), 80 °C, 6 h; [b]Reaction proceeded until 8 hrs; [c]C-C coupling product obtained; Isolated yield based on **6**.

A comparative study of Cu(0)/g-C_3N_4O with some previously reported catalysts employed in the Chan-Lam *N*-arylation of anilines with Phenylboronic acids is shown in Table **5.7**. It is evident that the present heterogeneous catalyst (Cu(0)/g-C_3N_4O) exhibits a decent TOF(h^{-1})/(TON).

Table **5.7** Comparative study of Cu(0)/g-C_3N_4O w.r.t. other benchmark catalysts for the Chan-Lam arylation of anilines with phenylboronic acids developed in recent years.[a]

Entry	Catalyst	TOF (h^{-1})/TON values
1	Cu@Fe_3O_4−TiO_2−L−dopa	16.3/48.4
2	Cu@PI−CO	18.0/144.3
3	$CoFe_2O_4$@SiO_2-NH_2-Furfural-Cu$(OAc)_2$	41.6/208
4	*N*−enriched GO/Cu	32/48
5	GO@AF−SB Cu	0.12/1.5
6	Cu(0)/g-C_3N_4O	65.3/392

[a]TON and TOF are calculated based on the amount of 'Cu' present on the surface

Combined with all the above mentioned merits, the developed material proves to be an efficient heterogeneous catalyst for Chan-Lam *N*-arylation under the optimized protocols.

5.3.7 *Conclusion*

We have successfully developed a Cu(0) NPs−based heterogeneous catalyst, Cu(0)/g-C_3N_4O to foster the Chan-Lam cross-coupling reaction of arylboronic acids with different nitrogen nucleophiles. The catalyst could be easily prepared in water and the preparation methodology involved a mild reducing agent. The π-bonded layered configuration of g-C_3N_4O was utilized to anchor a high loading of desired Cu(0) NPs on the surface and stabilized them up to five reaction cycles without significant oxidation. Heterogeneity of the easily synthesizable Cu(0)/g-C_3N_4O surpassed tedious workups and allowed easier separation from the reaction medium. Our protocol also had the advantage of achieving a base-free *N*−arylation of anilines and azoles in lesser catalytic quantities. We believe that our methodology has extended the scope of Chan-Lam *N*-arylation reaction through the introduction of a Cu(0) NPs catalytic route and has raised

its applicability in synthetic organic chemistry with a simple “heterogeneous” Cu(0)-catalytic system.

5.3.8 *Experimental section*

5.3.8.1 *General information*

All the chemicals used for the reactions were procured commercially and used without further purification. The progress of the reaction was monitored through thin layer chromatography on Merck Kieselgel Silica gel $60F_{254}$ plates using short wave UV light (λ=254 nm). The products were purified by column chromatography using Silica gel (60-120 mesh and 100-200 mesh). The identification of the purified products was done by NMR spectroscopy. The ^{1}H and ^{13}C NMR spectra were recorded on a 400 MHz JEOL NMR spectrometer (400 MHz for ^{1}H and 100 MHz for ^{13}C). Chemical shifts for both ^{1}H (δ_H) and ^{13}C (δ_C) NMR are assigned in parts per million (ppm) using TMS (0 ppm) as the internal reference and $CDCl_3$ and DMSO-d_6 as solvent ($CDCl_3$: δ_H = 7.25 ppm and δ_C = 77.1 ppm; DMSO-d_6: δ_H = 2.5 ppm, DMSO-d_6 absorbed water = 3.3 ppm and δ_C = 40.0 ppm). The multiplicities of the signals are assigned as: s = singlet, d = doublet, t = triplet, br = broad and m = multiplet. X-ray photoelectron spectroscopy (XPS) and auger measurements were carried out using a Thermo-Scientific ESCALAB Xi+ spectrometer having a monochromatic Al Kα X-ray source (1486.6 eV) and a spherical energy analyzer that operates in the CAE (constant analyzer energy) mode using the electromagnetic lens mode. The CAE for survey spectra is 100 eV and that for high-resolution spectra is 50 eV. TEM images were obtained on a JEM-2100 instrument with an accelerating voltage of 200 kV in 50 V steps. Prior to imaging, the materials were dispersed in ethanol by the ultrasonication method and the resultant ink was drop-cast on the carbon foil supported on the Cu grid. Infrared spectra were recorded with a Nicolet Impact I-410 FT-IR spectrometer as KBr diluted discs. UV-Vis experiments were performed with Shimadzu, UV-2550 spectrophotometer. The spectra were recorded by dispersing the catalyst sample in ethanol. p-XRD patterns of the samples were recorded on a Bruker AXS model D8 focus instrument with a Cu Kα (λ = 0.15418 nm) radiation source in the 2ϑ range of 10-80° with a step size of 0.05° s^{-1}. N_2 adsorption/desorption isotherms were collected on a Quantachrome Instrument (model: Nova 1000e) at −196

°C (liquid nitrogen temperature). The specific surface areas of the ECs were determined by the Brunauer-Emmett-Teller (BET) method using multi-point BET data at a relative pressure (P/P_o) region of 0.02-0.35. The sample was degassed at 100 °C for 5 hours prior to analysis. The pore size distribution of the ECs was determined following the Barrett-Joyner-Halenda (BJH) method in the same instrument. Yields of the kinetic study were determined by GC by comparison to anisole (internal standard) from appearance of product.

5.3.8.2 *Catalyst preparation*

a) Preparation of g-C_3N_4O

Guanidine hydrochloride (5 mmol, 0.475 g) dissolved in 10 mL distilled water was taken in a 250 mL conical flask. To this, 0.5 mL of polyethylene glycol (PEG) 400 was added under stirring at room temperature. The reaction flask was then placed in a microwave reactor at 600 W for 5 min and 2 min sequentially. The reaction flask was then allowed to cool and the resultant black/brown residue was diluted with 50 mL water. After that, the diluted residue was sonicated for 10 min and filtered to yield a yellow fluorescent solution of g-C_3N_4O (Figure **5.11a**). The g-C_3N_4O was obtained as a transparent yellow filtrate with a solid concentration of 22 mg/mL. Finally, the sample was lyophilized to obtain a light yellow solid of g-C_3N_4O (Figure **5.11b**).

b) Preparation of Cu(0)/g-C_3N_4O

In a 100 mL round bottomed flask, 0.1 g of $CuCl_2$ was taken and dissolved in 20 mL distilled water. To it, 25% aqueous ammonia was added dropwise under stirring, until a deep blue colouration persists in the solution. It was followed by dropwise addition of 0.1 mL PEG-400, 5 mL of the freshly prepared g-C_3N_4O and 0.2 g of ascorbic acid (saturated solution in water) sequentially to the stirring solution. The resultant reaction mixture was then refluxed for about 8 hours until a dark-red precipitate of Cu(0)/g-C_3N_4O was obtained. The precipitate was first separated by centrifugation and then washed with water (5 times) and ethanol (5 times). It was kept to dry in a vacuum desiccator overnight (Figure **5.11c**). The prepared Cu(0)/g-C_3N_4O was confirmed by different characterization techniques and employed in the Chan-Lam cross-coupling of a variety of *N*-nucleophiles.

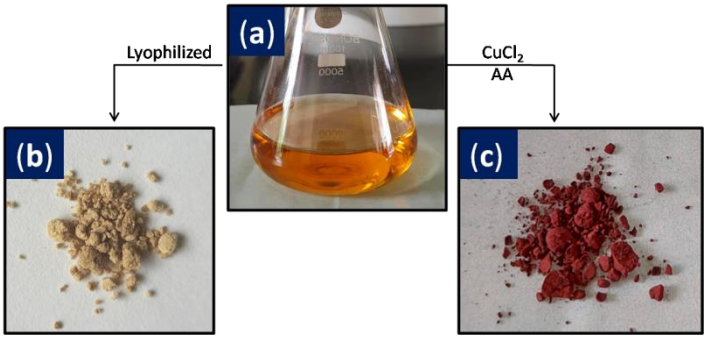

Figure **5.11** (**a**) bulk g-C_3N_4O; (**b**) Lyophilized g-C_3N_4O; (**c**) Cu(0)/g-C_3N_4O

5.3.8.3 *General experimental procedure*

A. *General procedure for N-arylation of anilines (**3**)*

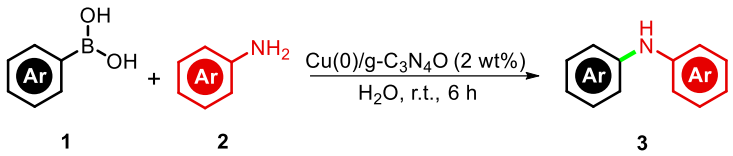

In a 50 mL round-bottomed flask with a magnetic stirring bead, 2 wt% (0.0023 g) of Cu(0)/g-C_3N_4O in 4 mL water was sonicated for 2 min. To it, phenylboronic acid, **1** (1 mmol) and aniline, **2** (0.8 mmol) were added. The reaction mixture was then stirred in open air at room temperature for 6-16 h. Progress of the reaction was monitored using TLC. After completion of reaction time, the resulting reaction mixture was extracted in ethyl acetate and concentrated on a rotary evaporator under reduced pressure. It was purified by column chromatography using ethyl acetate-hexane as an eluent to obtain the pure product (**3**).

B. *General procedure for N-arylation of imidazoles (**5**)*

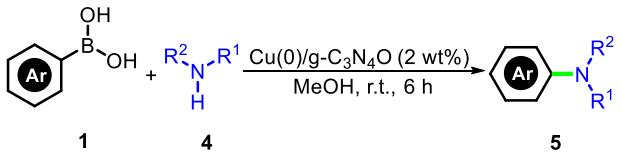

In a 50 mL round-bottomed flask with a magnetic stirring bead, 2 wt% (0.0021 g) of Cu(0)/g-C_3N_4O in 4 mL methanol was sonicated for 2 min. To it, phenylboronic acid, **1** (1 mmol) and azole, **4** (0.8 mmol) were added. The reaction mixture was then stirred in open air at room temperature for 6 h. Progress of the reaction was monitored using TLC. After completion of reaction time, the resulting reaction mixture was washed with

distilled water, extracted in ethyl acetate and concentrated under reduced pressure. It was purified by column chromatography using ethyl acetate-hexane as an eluent to obtain the pure product (**5**).

C. *General procedure for N-arylation of indoles (**7**)*

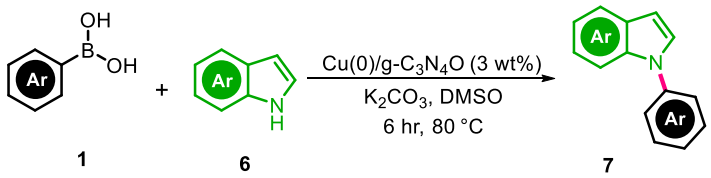

In a 50 mL round-bottomed flask with a magnetic stirring bead, 3 wt% (0.0032 g) of Cu(0)/g-C_3N_4O in 4 mL DMSO was sonicated for 2 min. To it, phenylboronic acid, **1** (1 mmol), indole, **6** (0.8 mmol) and K_2CO_3 (1 equiv., 1 mmol, 0.138 g) were added. The reaction mixture was then stirred under reflux conditions in a pre-heated oil bath at 80 °C. Progress of the reaction was monitored using TLC. After completion of reaction time, the resulting reaction mixture was washed with ice-cold water, extracted in ethyl acetate and concentrated under reduced pressure. It was purified by column chromatography using ethyl acetate-hexane as an eluent to obtain the pure product (**7**).

5.3.8.4 *Heterogeneity of Cu(0)/g-C_3N_4O*

To determine the active catalyst in the *N*-arylation of anilines, Cu(0)/g-C_3N_4O (2 wt%) was first sonicated in 4 mL water and then stirred for 3 hours. After 3 hours, the catalyst was separated through centrifugation and the supernatant reaction mixture was filtered. To the filtrate, 4−Methoxyphenylboronic acid, **1a** (1 mmol) and aniline, **2b** (0.8 mmol) was added and the reaction was allowed to stir under open air room temperature conditions for another 3 hours. GC-MS analysis of the crude reaction mixture detected ~1% of C-C coupling product. ICP−AAS analysis of the filtrate detected a leaching value of 1.6 ppm of Cu, which is insignificant. The above observations strongly support the heterogeneity of Cu(0)/g-C_3N_4O and that the *N*-arylation reaction takes place efficiently under heterogeneous catalysis.

5.3.8.5 *Recyclability test*

In a 100 mL round-bottomed flask with a magnetic stirring bead, Cu(0)/g-C_3N_4O (0.0135 g) in 30 mL water was sonicated for 10 min. To it, 4−Methoxyphenylboronic acid, **1a** (7

mmol, 1.0592 g) and aniline, **2a** (5.6 mmol, 525 µL) were added. The reaction mixture was then stirred in open air at room temperature for 6 h. After completion of reaction time, the Cu(0)/g-C_3N_4O was separated by centrifugation and the resulting supernatant reaction mixture was filtered and extracted in ethyl acetate and concentrated on a rotary evaporator under reduced pressure. The *N*-aryl product (**3a**) was isolated through column chromatography using ethyl acetate-hexane as an eluent in 93% yield. The recovered catalyst was washed with ethanol and left to dry in a vaccum dessicator overnight. For the subsequent runs, the recovered Cu(0)/g-C_3N_4O (which was left to dry) and the reagents were weighed accordingly. The recyclability tests were continued until the fifth run when there was a significant decrease in yield.

5.3.8.6 *Kinetic Study of the catalyst*

Kinetic study of the catalyst was done through GC analysis and the samples were prepared as per the general experimental procedure A and 4−Methoxyphenylboronic acid, **1a** (1 mmol) and aniline, **2b** (0.8 mmol) were taken as the substrates. Yields were determined by comparison to anisole (internal standard) from appearance of product.

5.3.9 ***NMR spectral analysis of N−aryl nitrile derivatives:***

5.3.9.1 *^{1}H and ^{13}C NMR spectral analysis of N−arylanilines (**3**)*

4−Methoxy-*N*-phenylaniline (**3a**)

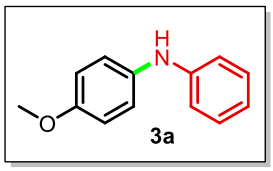

Synthesized as per the general experimental procedure A; obtained as a light yellow oil, Yield: 93% (148 mg); ^{1}H NMR (400 MHz, DMSO-d_6): δ_H (ppm) 3.66 (s, 3H), 6.66 (t, *J* = 8.0 Hz, 1H), 6.82 (d, *J* = 8.0 Hz, 2H), 6.88 (d, *J* = 8.0 Hz, 2H), 7.01 (d, *J* = 8.0 Hz, 2H), 7.11 (t, *J* = 8.0 Hz, 2H), 7.81 (br s, 1H); ^{13}C NMR (100 MHz, DMSO-d_6): δ_C (ppm) 55.7, 115.0, 115.2, 118.7, 120.8, 129.6, 136.6, 145.6, 154.3. Spectroscopic data was consistent with literature [37].

Diphenylamine (**3b**)

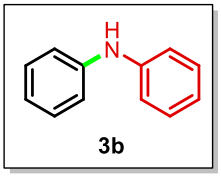

Synthesized as per the general experimental procedure A; obtained as a colourless solid, Yield: 81% (110 mg); ^{1}H NMR (400 MHz, DMSO-d_6): δ_H (ppm) 6.78 (t, J = 8.0 Hz, 2H), 7.05 (d, J = 8.0 Hz, 4H), 7.19 (d, J = 8.0 Hz, 4H), 8.14 (br s, 1H); ^{13}C NMR (100 MHz, DMSO-d_6): δ_C (ppm) 117.2, 120.1, 129.6, 143.9. Spectroscopic data was consistent with literature [37].

4−Ethyl-*N*-phenylaniline (**3c**)

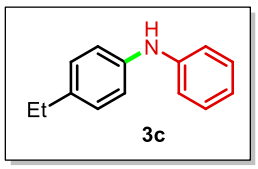

Synthesized as per the general experimental procedure A; obtained as a light yellow oil, Yield: 87% (137 mg); ^{1}H NMR (400 MHz, DMSO-d_6): δ_H (ppm) 1.11 (t, J = 8.0 Hz, 3H), 2.47-2.51 (m, 2H), 6.72 (t, J = 8.0 Hz, 1H), 6.97 (d, J = 8.0 Hz, 4H), 7.03 (d, J = 8.0 Hz, 2H), 7.15 (t, J = 8.0 Hz, 2H), 7.96 (br s, 1H); ^{13}C NMR (100 MHz, DMSO-d_6): δ_C (ppm) 16.3, 28.0, 116.4, 118.0, 119.5, 128.8, 129.6, 135.8, 141.4, 144.5. Spectroscopic data was consistent with literature [43].

N−phenylnapthalen-2-amine (**3d**)

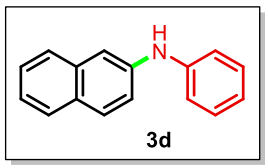

Synthesized as per the general experimental procedure A; obtained as a colourless solid, Yield: 75% (131 mg); ^{1}H NMR (400 MHz, DMSO-d_6): δ_H (ppm) 6.85 (t, J = 8.0 Hz, 1H), 7.18 (t, J = 8.0 Hz, 3H), 7.25 (t, J = 8.0 Hz, 3H), 7.33 (t, J = 8.0 Hz, 1H), 7.43 (br s, 1H), 7.64 (d, J = 8.0 Hz, 1H), 7.69-7.75 (m, 2H), 8.38 (s, 1H); ^{13}C NMR (100 MHz, DMSO-d_6): δ_C (ppm) 109.4, 117.8, 120.4, 120.7, 123.3, 126.7, 126.7, 127.9, 128.6, 129.3, 129.7, 134.9, 141.8, 143.5. Spectroscopic data was consistent with literature [35].

N−phenyl-3-(trifluoromethyl)aniline (**3e**)

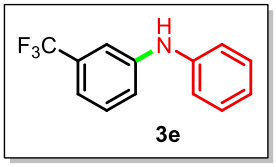

Synthesized as per the general experimental procedure A; obtained as a colourless solid, Yield: 78% (148 mg); ^{1}H NMR (400 MHz, DMSO-d_6): δ_H (ppm) 6.89 (t, J = 8.0 Hz, 1H), 7.03 (d, J = 8.0

Hz, 1H), 7.09 (d, J = 8.0 Hz, 2H), 7.23-7.28 (m, 4H), 7.37 (t, J = 8.0 Hz, 1H), 8.50 (br s, 1H); ^{13}C NMR (100 MHz, DMSO-d_6): δ_C (ppm) 112.0, 115.6, 118.7, 119.4, 121.7, 123.0, 123.4, 126.1, 129.8, 130.4, 130.8, 142.5, 145.2. Spectroscopic data was consistent with literature [32].

6−Methoxy-*N*-phenylpyridin-3-amine (**3f**)

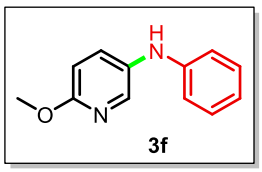

3f

Synthesized as per the general experimental procedure A; obtained as a yellow oil, Yield: 79% (126 mg), ^{1}H NMR (400 MHz, DMSO-d_6): δ_H (ppm) 3.77 (s, 3H), 6.68-6.74 (m, 2H), 6.85 (d, J = 8.0 Hz, 2H), 7.12-7.15 (m, 2H), 7.45-7.48 (m, 1H), 7.87 (br s, 1H), 7.92-7.97 (m, 1H); ^{13}C NMR (100 MHz, DMSO-d_6): δ_C (ppm) 53.5, 87.2, 111.0, 115.2, 119.2, 129.7, 132.1, 134.2, 137.9, 145.3, 159.0. Spectroscopic data was consistent with literature [86].

4−Bromo-*N*-phenylaniline (**3g**)

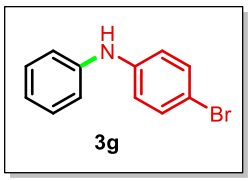

3g

Synthesized as per the general experimental procedure A; obtained as a yellow oil, Yield: 75% (149 mg), ^{1}H NMR (400 MHz, DMSO-d_6): δ_H (ppm) 6.82 (t, J = 8.0 Hz, 1H), 6.95-6.98 (m, 2H), 7.03 (d, J = 8.0 Hz, 2H), 7.20 (t, J = 8.0 Hz, 2H), 7.31 (d, J = 8.0 Hz, 2H), 8.28 (br s, 1H); ^{13}C NMR (100 MHz, DMSO-d_6): δ_C (ppm) 110.5, 117.8, 118.5, 120.9, 129.7, 132.3, 143.1, 143.5. Spectroscopic data was consistent with literature [28].

2−Bromo-*N*-phenylaniline (**3h**)

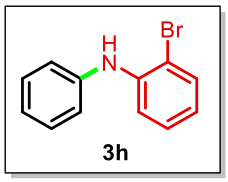

3h

Synthesized as per the general experimental procedure A; obtained as a light yellow oil, Yield: 72% (143 mg); ^{1}H NMR (400 MHz, DMSO-d_6): δ_H (ppm) 6.79-6.85 (m, 2H), 6.99 (d, J = 8.0 Hz, 2H), 7.17-7.23 (m, 4H), 7.46 (br s, 1H), 7.55 (d, J = 8.0 Hz, 1H); ^{13}C NMR (100 MHz, DMSO-d_6): δ_C (ppm) 114.8, 118.4, 120.0, 121.1, 123.0, 128.9, 129.6, 133.7, 141.9, 143.7. Spectroscopic data was consistent with literature [43].

Bis(4−methoxyphenyl)amine (**3i**)

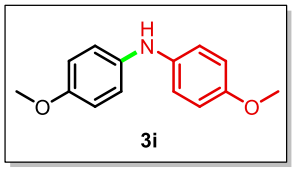

Synthesized as per the general experimental procedure A; obtained as a colourless solid, Yield: 85% (156 mg); ^{1}H NMR (400 MHz, DMSO-d_6): δ_H (ppm) 3.64 (s, 6H), 6.77 (d, J = 8.0 Hz, 4H), 6.89 (d, J = 8.0 Hz, 4H), 7.48 (br s, 1H); ^{13}C NMR (100 MHz, DMSO-d_6): δ_C (ppm) 55.7, 115.0, 118.5, 138.5, 153.3. Spectroscopic data was consistent with literature [85].

4−Methoxy-*N*-phenylaniline (**3j**)

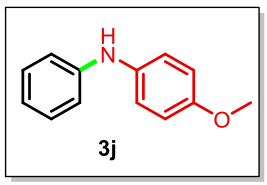

Synthesized as per the general experimental procedure A; obtained as a colourless solid, Yield: 80% (127 mg); ^{1}H NMR (400 MHz, DMSO-d_6): δ_H (ppm) 3.67 (s, 3H), 6.66 (t, J = 8.0 Hz, 1H), 6.81-6.88 (m, 5H), 7.00 (d, J = 8.0 Hz, 2H), 7.11 (t, J = 8.0 Hz, 2H), 7.77 (br s, 1H); ^{13}C NMR (100 MHz, DMSO-d_6): δ_C (ppm) 55.7, 115.0, 115.3,118.7, 120.9, 129.6, 136.6, 145.6, 154.3. Spectroscopic data was consistent with literature [12].

N-(4−methoxyphenyl)-2,4-dimethylaniline (**3k**)

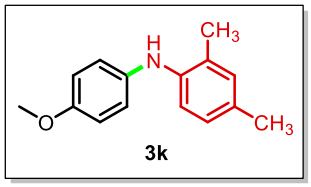

Synthesized as per the general experimental procedure A; obtained as a colourless liquid, Yield: 55% (100 mg); ^{1}H NMR (400 MHz, DMSO-d_6): δ_H (ppm) 2.10 (s, 3H), 2.15 (s, 3H), 3.64 (s, 3H), 6.74 (s, 1H), 6.79 (t, J = 8.0 Hz, 4H), 6.84-6.87 (m, 2H), 6.90 (br s, 1H); ^{13}C NMR (100 MHz, DMSO-d_6): δ_C (ppm) 18.4, 20.7, 55.6, 114.9, 118.0, 119.3, 127.3, 128.2, 129.6, 131.8, 138.8, 140.8, 153.4. Spectroscopic data was consistent with literature [87-88].

N–Benzyl-4-methoxyaniline (**3l**)

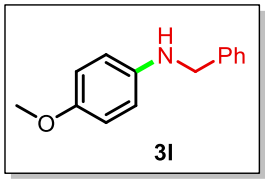

Synthesized as per the general experimental procedure A; obtained as a yellow oil, Yield: 72% (122 mg); ^{1}H NMR (400 MHz, DMSO-d_6): δ_H (ppm) 3.57 (s, 3H), 4.16 (s, 2H), 5.74 (br s, 1H), 6.49 (d, J = 8.0 Hz, 2H), 6.62-6.65 (m, 2H), 7.15-7.18 (m, 1H), 7.25 (d, J = 8.0 Hz, 2H), 7.30 (t, J = 8.0 Hz, 2H); ^{13}C NMR (100 MHz, DMSO-d_6): δ_C (ppm) 47.8, 55.8, 113.8, 115.0, 127.0, 127.7, 128.7, 141.0, 143.4, 151.2. Spectroscopic data was consistent with literature [89].

N–(4–methoxyphenyl)pyridin-2-amine (**3m**)

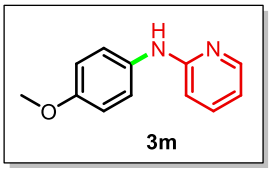

Synthesized as per the general experimental procedure A; obtained as a light yellow oil, Yield: 70% (112 mg); ^{1}H NMR (400 MHz, DMSO-d_6): δ_H (ppm) 3.66 (s, 3H), 6.59-6.62 (m, 1H), 6.68 (d, J = 8.0 Hz, 1H), 6.81 (d, J = 8.0 Hz, 2H), 7.44 (t, J = 8.0 Hz, 1H), 7.49 (d, J = 8.0 Hz, 2H), 8.03 (d, J = 8.0 Hz, 1H), 8.72 (br s, 1H); ^{13}C NMR (100 MHz, DMSO-d_6): δ_C (ppm) 55.7, 110.3, 114.0, 114.3, 120.5, 135.3, 137.5, 147.7, 154.1, 156.8. Spectroscopic data was consistent with literature [90].

4–Nitro-*N*-phenylaniline (**3n**)

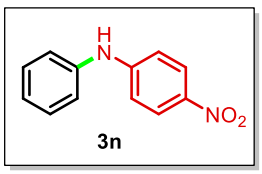

Synthesized as per the general experimental procedure A; obtained as a yellow solid, Yield: 65% (111 mg); ^{1}H NMR (400 MHz, DMSO-d_6): δ_H (ppm) 7.00-7.04 (m, 2H), 7.07 (d, J = 8.0 Hz, 1H), 7.20 (d, J = 8.0 Hz, 2H), 7.34 (t, J = 8.0 Hz, 2H), 8.04 (d, J = 8.0 Hz, 2H), 9.25 (br s, 1H); ^{13}C NMR (100 MHz, DMSO-d_6): δ_C (ppm) 113.7, 121.2, 123.9, 126.7, 130.0, 138.3, 140.5, 151.3. Spectroscopic data was consistent with literature [37].

5.3.9.2 *^{1}H and ^{13}C NMR spectral analysis of N-arylazoles (**5**)*

1−(4−Methoxyphenyl)-4-methyl-1*H*-imidazole (**5a**)

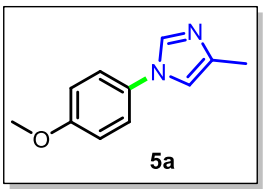

Synthesized as per the general experimental procedure B; obtained as a light yellow oil, Yield: 91% (136 mg); ^{1}H NMR (400 MHz, DMSO-d_6): δ_H (ppm) 2.12 (s, 3H), 3.72 (s, 3H), 6.97 (d, J = 8.0 Hz, 2H), 7.24 (s, 1H), 7.43 (d, J = 8.0 Hz, 2H), 7.96 (s, 1H); ^{13}C NMR (100 MHz, DMSO-d_6): δ_C (ppm) 14.0, 55.8, 114.9, 115.2, 122.0, 130.9, 135.1, 138.5, 158.2. Spectroscopic data was consistent with literature [91].

1−(4−Methoxyphenyl)-2-methyl-1*H*-imidazole (**5b**)

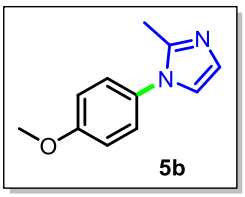

Synthesized as per the general experimental procedure B; obtained as a light yellow oil, Yield: 89% (134 mg); ^{1}H NMR (400 MHz, $CDCl_3$): δ_H (ppm) 2.28 (s, 3H), 3.81 (s, 3H), 6.91-6.95 (m, 4H), 7.14-7.17 (m, 2H); ^{13}C NMR (100 MHz, DMSO-d_6): δ_C (ppm) 13.8, 55.9, 115.0, 121.5, 127.1, 127.4, 131.0, 144.3, 159.2. Spectroscopic data was consistent with literature [92].

1−Phenyl−1*H*-imidazole (**5c**)

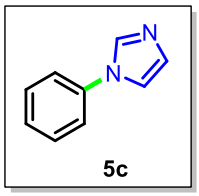

Synthesized as per the general experimental procedure B; obtained as a colourless oil, Yield: 70% (81 mg); ^{1}H NMR (400 MHz, $CDCl_3$): δ_H (ppm) 7.37-7.40 (m, 4H), 7.48 (t, J = 8 Hz, 2H), 7.94 (s, 1H), 8.07 (d, J = 8 Hz, 1H); ^{13}C NMR (100 MHz, DMSO-d_6): δ_C (ppm) 118.5, 120.8, 127.3, 130.3, 130.4, 136.0, 137.4. Spectroscopic data was consistent with literature [30].

1−Phenyl−2−methyl−1*H*−imidazole (**5d**)

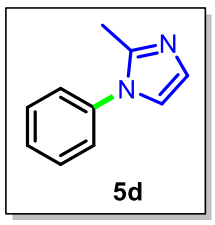

Synthesized as per the general experimental procedure B; obtained as a light yellow oil, Yield: 76% (96 mg); ^{1}H NMR (400 MHz, $CDCl_3$): δ_H (ppm) 2.32 (s, 3H), 6.96-6.99 (m, 2H), 7.24 (d, J = 8.0 Hz, 2H), 7.38 (t, J = 8.0 Hz, 1H), 7.44 (t, J = 8.0 Hz, 2H); ^{13}C NMR (100 MHz, DMSO-d_6): δ_C (ppm) 13.8, 121.2, 125.5, 127.6, 128.3,

130.0, 138.0, 144.2. Spectroscopic data was consistent with literature [91-92].

4−Methyl-1-phenyl-1*H*-imidazole (**5e**)

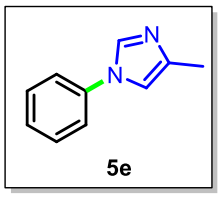

Synthesized as per the general experimental procedure B; obtained as a light yellow oil, Yield: 79% (99 mg); ^{1}H NMR (400 MHz, DMSO-d_6): δ_H (ppm) 2.12 (s, 3H), 7.27 (t, J = 8 Hz , 1H), 7.38 (s, 1H), 7.42-7.46 (m, 2H), 7.55 (d, J = 8 Hz, 2H), 8.09 (s, 1H); ^{13}C NMR (100 MHz, DMSO-d_6): δ_C (ppm) 14.1, 114.6, 120.3, 126.9, 130.3, 135.1, 137.5, 138.9. Spectroscopic data was consistent with literature [30].

1−(4−Fluorophenyl)-4-methyl-1*H*-imidazole (**5f**)

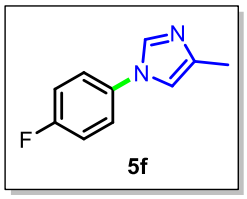

Synthesized as per the general experimental procedure B; obtained as a colourless oil, Yield: 88% (155 mg); ^{1}H NMR (400 MHz, DMSO-d_6): δ_H (ppm) 2.11 (s, 3H), 7.31 (d, J = 8.0 Hz, 2H), 7.36 (s, 1H), 7.60 (d, J = 8.0 Hz, 2H), 8.04 (s, 1H); ^{13}C NMR (100 MHz, DMSO-d_6): δ_C (ppm) 14.0, 114.9, 117.0, 122.5, 134.1, 135.3, 138.8, 162.0. Spectroscopic data was consistent with literature [93].

1−(3−Methylphenyl)-2-methyl-1*H*-imidazole (**5g**)

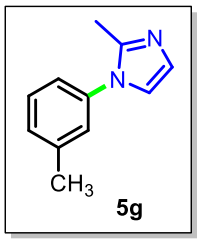

Synthesized as per the general experimental procedure B; obtained as a colourless oil, Yield: 83% (114 mg); ^{1}H NMR (400 MHz, $CDCl_3$): δ_H (ppm) 2.28 (s, 3H), 2.35 (s, 3H), 6.92-6.95 (m, 2H), 7.01 (d, J = 8.0 Hz, 2H), 7.16 (s, 1H), 7.28 (t, J = 8.0 Hz, 1H); ^{13}C NMR (100 MHz, DMSO-d_6): δ_C (ppm) 13.9, 21.2, 121.2, 122.6, 126.0, 127.6, 128.9, 129.7, 138.0, 139.7, 144.1. Spectroscopic data was consistent with literature [91].

1−(3−Nitrophenyl)-4-methyl-1*H*-imidazole (**5h**)

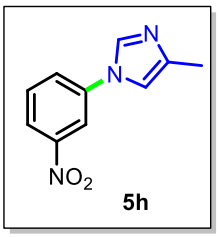

Synthesized as per the general experimental procedure B; obtained as a yellow solid, Yield: 76% (123 mg); ^{1}H NMR (400 MHz, DMSO-d_6): δ_H (ppm) 2.12 (s, 3H), 7.61 (s, 1H), 7.71 (t, J = 8.0 Hz, 1H), 8.03 (d, J = 8.0 Hz, 1H), 8.07 (d, J = 8.0 Hz, 1H), 8.25 (s, 1H), 8.35 (s, 1H); ^{13}C NMR (100 MHz, DMSO-d_6): δ_C (ppm) 14.0, 100.0, 114.8, 121.3, 126.3, 126.4, 131.7, 138.3, 149.2. Spectroscopic data was consistent with literature [94].

1−(2−Methylphenyl)-4-methyl-1*H*-imidazole (**5i**)

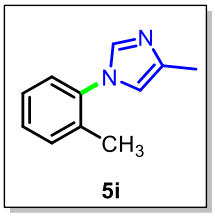

Synthesized as per the general experimental procedure B; obtained as a colourless oil, Yield: 80% (110 mg); ^{1}H NMR (400 MHz, $CDCl_3$): δ_H (ppm) 2.11 (s, 3H), 2.14 (s, 3H), 6.99 (s, 1H), 7.20 (d, J = 8.0 Hz, 1H), 7.27 (d, J = 8.0 Hz, 1H), 7.32 (t, J = 8.0 Hz, 2H), 7.62 (s, 1H); ^{13}C NMR (100 MHz, DMSO-d_6): δ_C (ppm)13.9, 17.9, 117.5, 126.6, 127.4, 128.7, 131.6, 133.4, 137.1, 137.6. Spectroscopic data was consistent with literature [93].

3−(4−Methyl-1*H*-imidazol-1-yl)benzonitrile (**5j**)

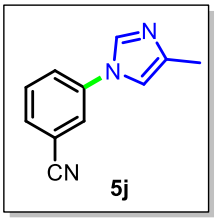

Synthesized as per the general experimental procedure B; obtained as a light yellow oil, Yield: 72% (105 mg); ^{1}H NMR (400 MHz, $CDCl_3$): δ_H (ppm) 2.36 (s, 3H), 7.00-7.05 (m, 2H), 7.54 (d, J = 8.0 Hz, 1H), 7.59 (s, 1H), 7.63 (d, J = 8.0 Hz, 1H), 7.71 (d, J = 8.0 Hz, 1H); ^{13}C NMR (100 MHz, DMSO-d_6) δ_C (ppm) 14.1, 113.0, 118.4, 128.0, 129.1, 130.5, 131.3, 132.1, 138.9. Spectroscopic data was consistent with literature [95].

1−Phenyl−1*H*−benzo[*d*]imidazole (**5k**)

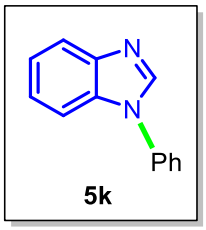

5k

Synthesized as per the general experimental procedure B; obtained as a colourless oil, Yield: 75% (116 mg); ^{1}H NMR (400 MHz, DMSO-d_6): δ_H (ppm) 7.25-7.27 (m, 2H), 7.42 (d, J = 8.0 Hz, 1H), 7.51-7.55 (m, 3H), 7.59 (t, J = 8.0 Hz, 2H), 7.76-7.79 (m, 1H), 8.52 (s, 1H); ^{13}C NMR (100 MHz, DMSO-d_6) δ_C (ppm) 111.1, 120.5, 123.0, 124.1, 128.1, 130.5, 133.6, 136.5, 143.8, 144.4. Spectroscopic data was consistent with literature [30].

1−Phenyl−1*H*−benzo[*d*]imidazol-2-amine (**5l**)

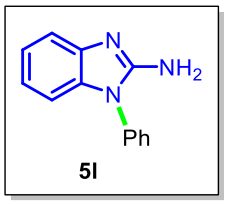

5l

Synthesized as per the general experimental procedure B; obtained as a colourless solid, Yield: 78% (130 mg); ^{1}H NMR (400 MHz, $CDCl_3$): δ_H (ppm) 5.88 (br s, 2H), 6.96-7.03 (m, 2H), 7.14 (t, J = 8.0 Hz, 1H), 7.41 (d, J = 8.0 Hz, 1H), 7.45 (d, J = 8.0 Hz, 2H), 7.50 (d, J = 8.0 Hz, 1H), 7.56-7.59 (m, 2H); ^{13}C NMR (100 MHz, $CDCl_3$) δ_C (ppm) 108.6, 115.8, 120.3, 122.4, 126.7, 129.1, 130.5, 134.6, 140.9. Spectroscopic data was consistent with literature [34].

N−1−diphenyl−1*H*−benzo[*d*]imidazol−2−amine (**5m**)

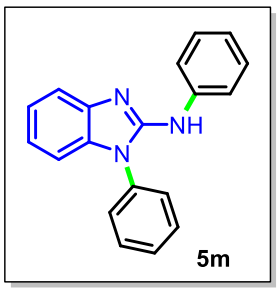

5m

Synthesized as per the general experimental procedure A; obtained as a colourless solid, Yield: 60% (103 mg); ^{1}H NMR (400 MHz, DMSO-d_6): δ_H (ppm) 6.89 (t, J = 8.0 Hz, 2H), 6.97 (t, J = 8.0 Hz, 1H), 7.08 (t, J = 8.0 Hz, 1H), 7.24 (t, J = 8.0 Hz, 2H), 7.43 (d, J = 8.0 Hz, 1H), 7.52 (t, J = 8.0 Hz, 3H), 7.62 (t, J = 8.0 Hz, 2H), 7.75 (d, J = 8.0 Hz, 2H), 8.61 (br s, 1H); ^{13}C NMR (100 MHz, DMSO-d_6) δ_C (ppm) 108.7, 117.0, 118.8, 120.9, 121.6, 122.2, 127.9, 128.9, 129.1, 130.7, 135.2, 141.3, 142.4, 150.3. Spectroscopic data was consistent with literature [96].

5.3.9.3 *^{1}H and ^{13}C NMR spectral analysis of N-arylindoles (**7**)*

1−Phenyl−1*H*−indole (**7a**)

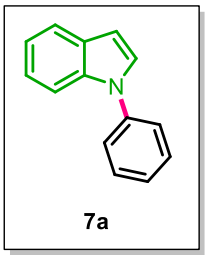

Synthesized as per the general experimental procedure C; obtained as a colourless solid, Yield: 87% (134 mg); ^{1}H NMR (400 MHz, DMSO-d_6): δ_H (ppm) 6.67 (d, J = 8.0 Hz, 1H), 7.10 (t, J = 8.0 Hz, 1H), 7.15 (t, J = 8.0 Hz, 1H), 7.32-7.37 (m, 1H), 7.50-7.53 (m, 5H), 7.59 (d, J = 8.0 Hz, 1H), 7.63 (d, J = 8.0 Hz, 1H); ^{13}C NMR (100 MHz, DMSO-d_6) δ_C (ppm) 104.0, 110.8, 120.7, 121.5, 122.8, 124.3, 126.9, 128.9, 129.6, 130.3, 135.6, 139.6. Spectroscopic data was consistent with literature [97].

5−Nitro−1−Phenyl−1*H*−indole (**7b**)

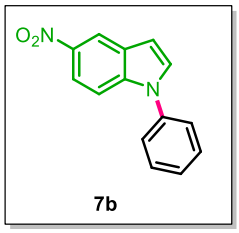

Synthesized as per the general experimental procedure C; obtained as a yellow solid, Yield: 82% (156 mg); ^{1}H NMR (400 MHz, DMSO-d_6): δ_H (ppm) 6.93 (d, J = 8.0 Hz, 1H), 7.41-7.45 (m, 1H), 7.53-7.57 (m, 5H), 7.84 (d, J = 8.0 Hz, 1H), 7.98 (d, J = 8.0 Hz, 1H), 8.59 (d, J = 8.0 Hz, 1H); ^{13}C NMR (100 MHz, DMSO-d_6) δ_C (ppm) 106.2, 111.3, 118.0, 118.4, 124.8, 128.0, 128.9, 130.5, 132.9, 138.3, 138.5, 141.9. Spectroscopic data was consistent with literature [97].

3−Methyl−1−Phenyl−1*H*−indole (**7c**)

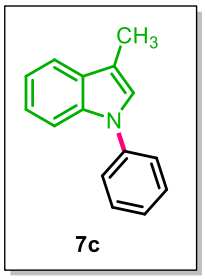

Synthesized as per the general experimental procedure C; obtained as a colourless oil, Yield: 85% (141 mg); ^{1}H NMR (400 MHz, DMSO-d_6): δ_H (ppm) 2.28 (s, 3H), 7.09 (t, J = 8.0 Hz, 1H), 7.15 (t, J = 8.0 Hz, 1H), 7.29-7.33 (m, 1H), 7.39 (s, 1H), 7.49-7.52 (m, 5H), 7.56 (d, J = 8.0 Hz, 1H); ^{13}C NMR (100 MHz, DMSO-d_6) δ_C (ppm) 9.9, 110.7, 112.5, 119.1, 119.6, 120.2, 121.6, 122.9, 123.8, 126.2, 130.0, 130.3, 135.6, 139.7, 157.1. Spectroscopic data was consistent with literature [98].

2−Methyl−1−Phenyl−1*H*−indole (**7d**)

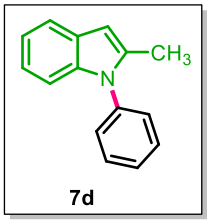

Synthesized as per the general experimental procedure C; obtained as a colourless oil, Yield: 75% (124 mg); ^{1}H NMR (400 MHz, DMSO-d_6): δ_H (ppm) 2.23 (s, 3H), 6.38 (s, 1H), 6.96-7.01 (m, 3H), 7.39 (d, *J* = 8.0 Hz, 2H), 7.46 (t, *J* = 8.0 Hz, 2H), 7.56 (t, *J* = 8.0 Hz, 2H); ^{13}C NMR (100 MHz, DMSO-d_6) δ_C (ppm) 13.6, 101.7, 110.1, 119.9, 120.3, 121.5, 128.1, 128.3, 130.2, 137.2, 137.7, 138.02. Spectroscopic data was consistent with literature [97].

7−Bromo−1−(*m*−tolyl)−1*H*−indole (**7e**)

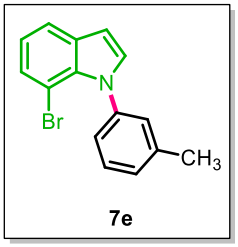

Synthesized as per the general experimental procedure C; obtained as a yellow oil, Yield: 70% (160 mg); ^{1}H NMR (400 MHz, $CDCl_3$): δ_H (ppm) 2.41 (s, 3H), 6.63 (d, *J* = 8.0 Hz, 1H), 6.99 (t, *J* = 8.0 Hz, 1H), 7.17-7.20 (m, 3H), 7.23 (s, 1H), 7.31 (d, *J* = 8.0 Hz, 1H), 7.36 (d, *J* = 8.0 Hz, 1H), 7.62 (d, *J* = 8.0 Hz, 1H); ^{13}C NMR (100 MHz, $CDCl_3$) δ_C (ppm) 21.4, 102.8, 104.4, 120.4, 121.1, 125.7, 127.3, 128.1, 128.80, 129.3, 131.5, 132.0, 133.4, 138.3, 139.6.

5−Bromo−1−(4−methoxyphenyl)−1*H*−indole (**7f**)

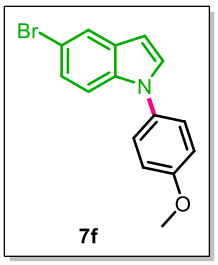

Synthesized as per the general experimental procedure C; obtained as a light yellow oil, Yield: 80% (193 mg); ^{1}H NMR (400 MHz, DMSO-d_6): δ_H (ppm) 3.77 (s, 3H), 6.61 (d, *J* = 8.0 Hz, 1H), 7.06 (d, *J* = 8.0 Hz, 2H), 7.22 (d, *J* = 8.0 Hz, 1H), 7.30-7.33 (m, 1H), 7.40 (d, *J* = 8.0 Hz, 2H), 7.55 (d, *J* = 8.0 Hz, 1H), 7.79 (d, *J* = 8.0 Hz, 1H); ^{13}C NMR (100 MHz, DMSO-d_6) δ_C (ppm) 56.0, 102.9, 112.7, 112.9, 115.4, 123.5, 125.0, 126.0, 130.7, 131.0, 132.06, 134.8, 158.5. Spectroscopic data was consistent with literature [99].

3−Methyl−1−(3−(trifluoromethyl)−phenyl)−1*H*−indole (**7g**)

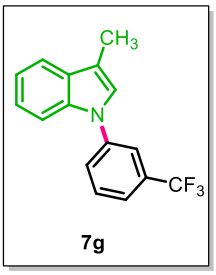

7g

Synthesized as per the general experimental procedure C; obtained as a colourless oil, Yield: 65% (143 mg); ^{1}H NMR (400 MHz, DMSO-d_6): δ_H (ppm) 2.28 (s, 3H), 7.10-7.13 (m, 1H), 7.17-7.20 (m, 1H), 7.30-7.37 (m, 1H), 7.51 (d, J = 8.0 Hz, 2H), 7.56-7.62 (m, 2H), 7.80 (s, 1H), 7.86 (d, J = 8.0 Hz, 1H); ^{13}C NMR (100 MHz, DMSO-d_6) δ_C (ppm) 9.8, 113.4, 123.2, 124.1, 125.3, 126.0, 126.2, 127.6, 129.9, 130.2, 130.6, 131.6, 135.5, 140.1, 140.4, 156.9. Spectroscopic data was consistent with literature [98].

4−(3−Methyl−1*H*−indol−1−yl)benzonitrile (**7h**)

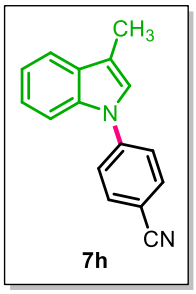

7h

Synthesized as per the general experimental procedure C; obtained as a light yellow oil, Yield: 60% (111 mg); ^{1}H NMR (400 MHz, DMSO-d_6): δ_H (ppm) 2.17 (s, 3H), 5.39 (s, 2H), 6.94 (t, J = 8.0 Hz, 1H), 7.07 (t, J = 8.0 Hz, 1H), 7.18 (s, 1H), 7.31 (d, J = 8.0 Hz, 1H), 7.41 (d, J = 8.0 Hz, 1H), 7.45 (d, J = 8.0 Hz, 1H), 7.57 (d, J = 8.0 Hz, 1H); ^{13}C NMR (100 MHz, DMSO-d_6) δ_C (ppm) 10.0, 109.1, 110.4, 111.7, 118.6, 119.0, 119.2, 121.7, 125.3, 126.9, 128.9, 136.4, 136.8. Spectroscopic data was consistent with literature [100].

1−(4−Ethylphenyl)-1*H*-indole (**7i**)

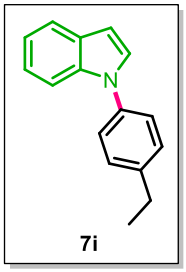

7i

Synthesized as per the general experimental procedure C; obtained as a colourless oil, Yield: 88% (155 mg); ^{1}H NMR (400 MHz, DMSO-d_6): δ_H (ppm) 1.20 (t, J = 8.0 Hz, 3H), 2.65 (q, J = 8.0 Hz, 2H), 6.64 (d, J = 8.0 Hz, 1H), 7.07 (t, J = 8.0 Hz, 1H), 7.14 (t, J = 8.0 Hz, 1H), 7.36 (d, J = 8.0 Hz, 2H), 7.43-7.49 (m, 3H), 7.57 (d, J = 8.0 Hz, 1H), 7.61 (d, J = 8.0 Hz, 1H); ^{13}C NMR (100 MHz, DMSO-d_6) δ_C (ppm) 16.1, 28.2, 103.7, 110.8, 120.6, 121.4, 122.7, 124.3, 129.0, 129.4, 135.6, 137.3, 142.6. Spectroscopic data was consistent with literature [101].

5.3.10 *Representative ^{1}H and ^{13}C NMR spectra of N-aryl derivatives:*

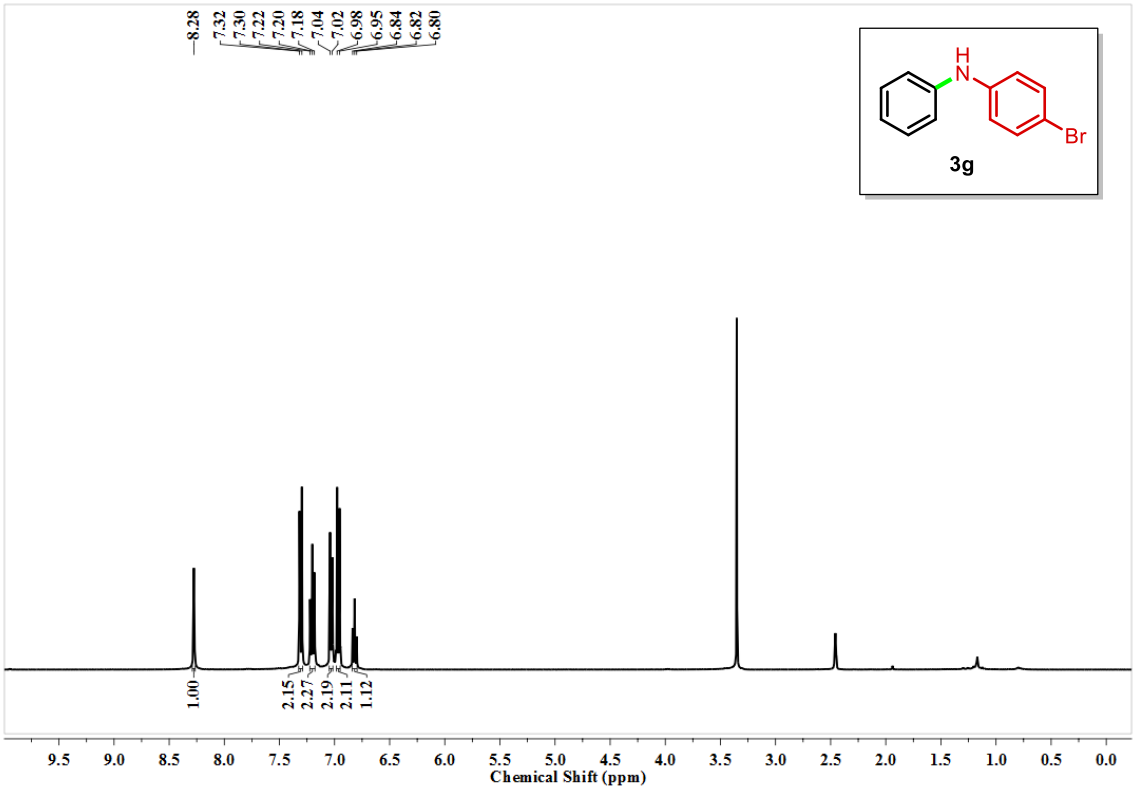

Figure **5.12** ^{1}H NMR spectrum of **3g** in DMSO−d_6 (400 MHz, 298 K)

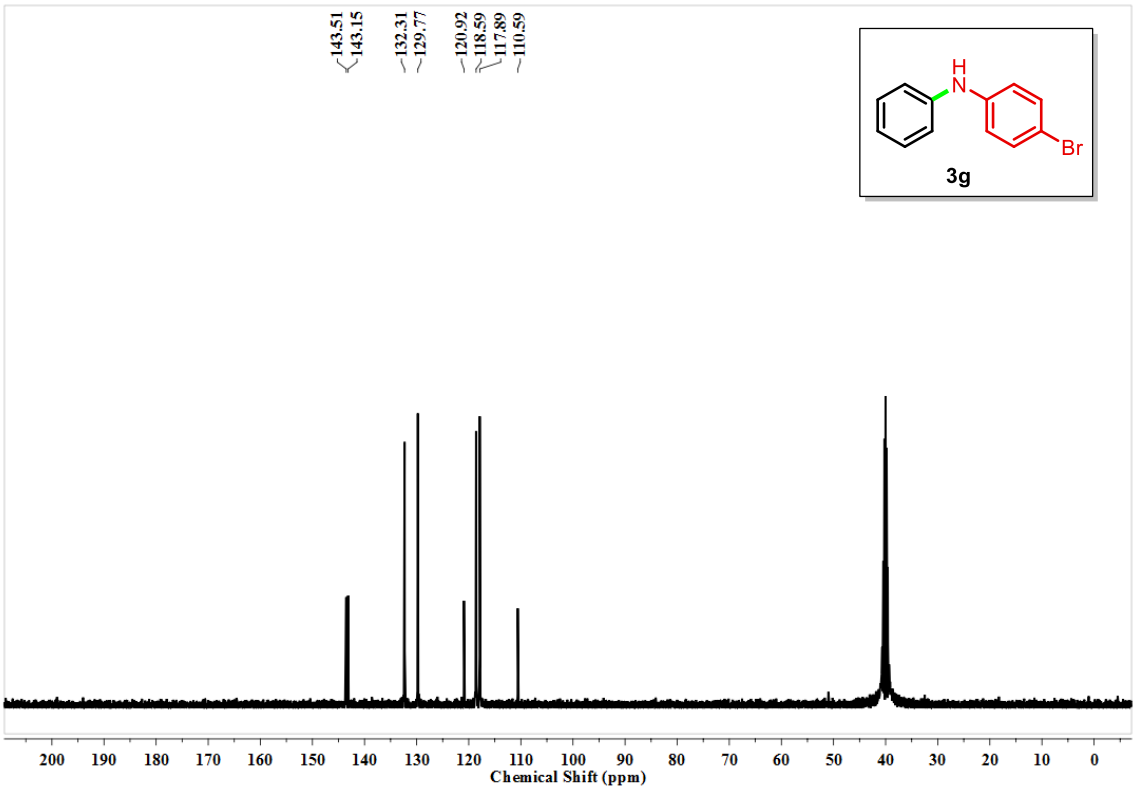

Figure **5.13** ^{13}C NMR spectrum of **3g** in DMSO−d_6 (100 MHz, 298 K)

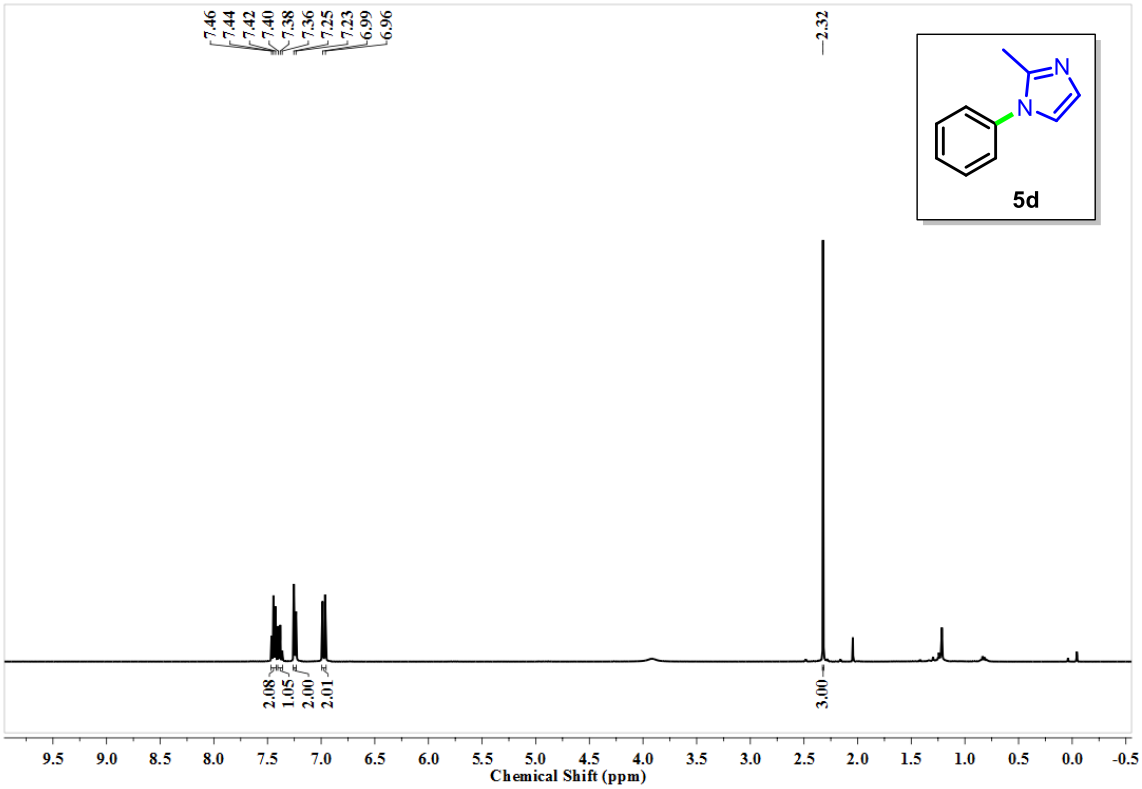

Figure **5.14** ^{1}H NMR spectrum of **5d** in DMSO−d_6 (400 MHz, 298 K)

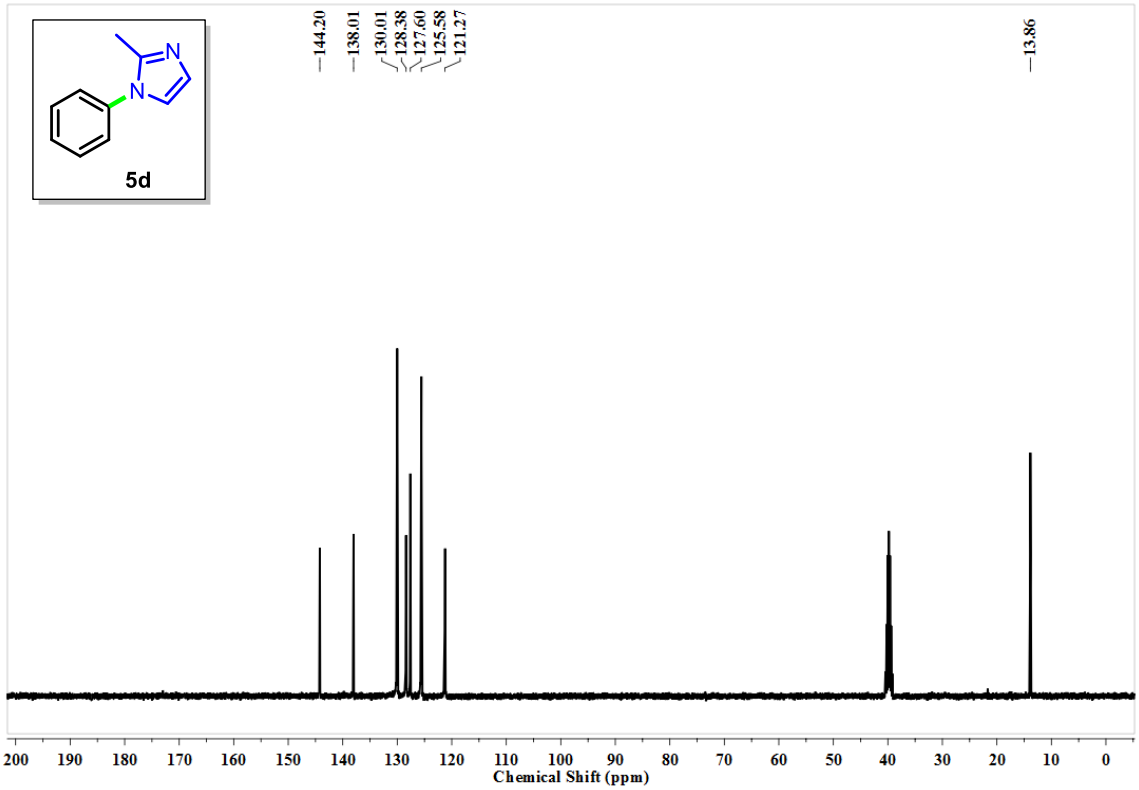

Figure **5.15** ^{13}C NMR spectrum of **5d** in DMSO−d_6 (100 MHz, 298 K)

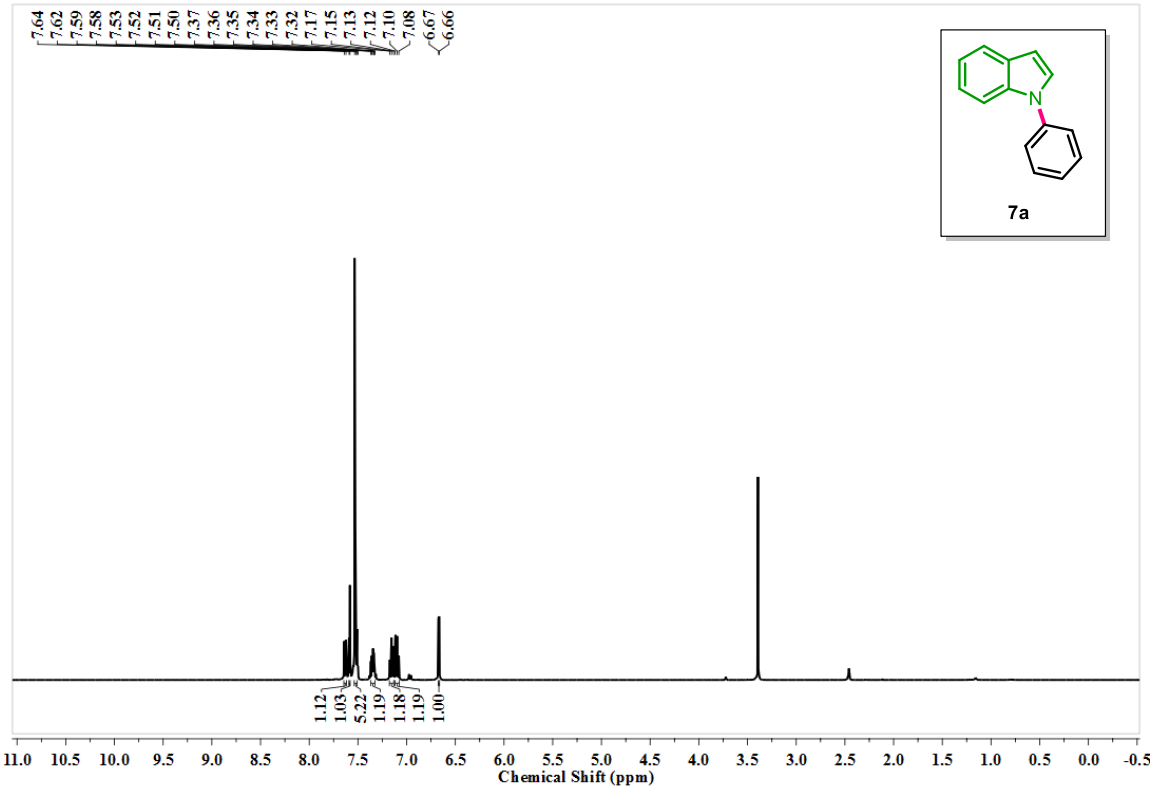

Figure **5.16** ^{1}H NMR spectrum of **7a** in DMSO−d_6 (400 MHz, 298 K)

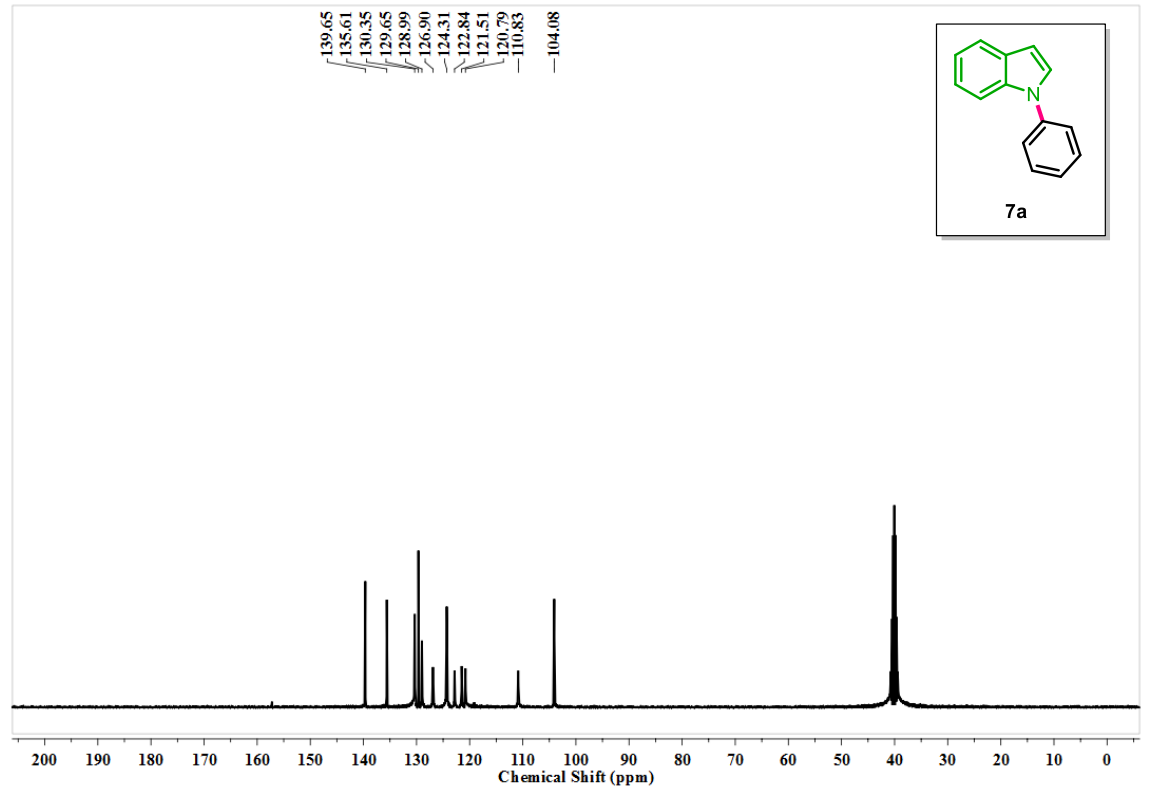

Figure **5.17** ^{13}C NMR spectrum of **7a** in DMSO−d_6 (100 MHz, 298 K)

5.4 *Bibliography*

[1] Chan, D. M., Monaco, K. L., Wang, R. P., and Winters, M. P. New *N*-and *O*-arylations with Phenylboronic acids and Cupric acetate. *Tetrahedron Letters*, 39(19):2933-2936, 1998.

[2] Evans, D. A., Katz, J. L., and West, T. R. Synthesis of Diaryl Ethers through the Copper-Promoted Arylation of Phenols with Arylboronic Acids. An Expedient Synthesis of Thyroxine. *Tetrahedron Letters*, 39(19):2937-2940, 1998. Prof. Evans' group found out about the discovery of this reaction on a National Organic Symposium poster and became interested in the *O*-arylation because of his long interest in vancomycin total synthesis.

[3] Lam, P. Y., Clark, C. G., Saubern, S., Adams, J., Winters, M. P., Chan, D. M., and Combs, A. New Aryl/Heteroaryl C−N Bond Cross-Coupling Reactions *via* Arylboronic Acid/Cupric Acetate Arylation. *Tetrahedron Letters*, 39(19):2941-2944, 1998.

[4] Lam, P. Y., Vincent, G., Clark, C. G., Deudon, S., and Jadhav, P. K. Copper-Catalyzed General C−N and C−O Bond Cross-Coupling with Arylboronic Acid. *Tetrahedron Letters*, 42(20):3415-3418, 2001.

[5] Shi, Z., Zhang, C., Tang, C., and Jiao, N. Recent Advances in Transition-Metal Catalyzed Reactions Using Molecular Oxygen as the Oxidant. *Chemical Society Reviews*, 41(8):3381-3430, 2012.

[6] Ley, S. V., and Thomas, A. W. Modern Synthetic Methods for Copper-Mediated C(aryl)−O, C(aryl)−N, and C(aryl)−S Bond Formation. *Angewandte Chemie International Edition*, 42(44):5400-5449, 2003.

[7] Chan, D. M., and Lam, P. Y. Boronic Acids, In Hall, D. G., editor, *Boronic Acids: Preparation and Applications in Organic Synthesis and Medicine,* pages 205-240, Wiley-VCH, 2005.

[8] Qiao, J. X., and Lam, P. Y. Copper-Promoted Carbon-Heteroatom Bond Cross-Coupling with Boronic Acids and Derivatives. *Synthesis*, 2011(06):829-856, 2011.

[9] Rao, K. S., and Wu, T. S. Chan-Lam Coupling Reactions: Synthesis of Heterocycles. *Tetrahedron* (Oxford. Print), 68(38):7735-7754, 2012.

[10] Tian, Y. M., Guo, X. N., Wu, Z., Friedrich, A., Westcott, S. A., Braunschweig, H., Radius, U., and Marder, T. B. Ni-Catalyzed Traceless, Directed C3−Selective C−H Borylation of Indoles. *Journal of the American Chemical Society*, 142(30):13136-13144, 2020.

[11] Silva, M. P., Saraiva, L., Pinto, M., and Sousa, M. E. Boronic Acids and their Derivatives in Medicinal Chemistry: Synthesis and Biological Applications. *Molecules*, 25(18):4323, 2020.

[12] Antilla, J. C., and Buchwald, S. L. Copper-Catalyzed Coupling of Arylboronic Acids and Amines. *Organic Letters*, 3(13):2077-2079, 2001.

[13] Herradura, P. S., Pendola, K. A., and Guy, R. K. Copper-Mediated Cross-Coupling of Aryl Boronic Acids and Alkyl Thiols. *Organic Letters*, 2(14):2019-2022, 2000.

[14] Silva, H., Fu, H., Jiang, Y., and Zhao, Y. Easy Copper−Catalyzed Synthesis of Primary Aromatic Amines by Couplings Aromatic Boronic Acids with Aqueous Ammonia at Room Temperature. *Angewandte Chemie*, 121(6):1134-1136, 2009.

[15] Li, J., Benard, S., Neuville, L., and Zhu, J. Copper Catalyzed *N*-arylation of Amidines with Aryl Boronic Acids and One-Pot Synthesis of Benzimidazoles by a Chan-Lam-Evans *N*-arylation and C-H Activation/C-N Bond Forming Process. *Organic Letters*, 14(23):5980-5983, 2012.

[16] Gao, X., Fu, H., Qiao, R., Jiang, Y., and Zhao, Y. Copper-Catalyzed Synthesis of Primary Arylamines *via* Cascade Reactions of Aryl Halides with Amidine Hydrochlorides. *The Journal of Organic Chemistry*, 73(17):6864-6866, 2008.

[17] Uemura, T., and Chatani, N. Copper Salt Catalyzed Addition of Arylboronic Acids to Azodicarboxylates. *The Journal of Organic Chemistry*, 70(21):8631-8634, 2005.

[18] Wolter, M., Klapars, A., and Buchwald, S. L. Synthesis of *N*-aryl Hydrazides by Copper-Catalyzed Coupling of Hydrazides with Aryl Iodides. *Organic Letters*, 3(23):3803-3805, 2001.

[19] Orooji, Y., Pakzad, K., Nasrollahzadeh, M., and Tajbakhsh, M. Novel Magnetic Lignosulfonate-Supported Pd-complex as an Efficient Nanocatalyst for *N*-arylation of 4-Methylbenzenesulfonamide. *International Journal of Biological Macromolecules*, 182:564-573, 2021.

[20] Nasrollahzadeh, M., Nezafat, Z., Pakzad, K., and Ahmadpoor, F. Synthesis of Magnetic Chitosan Supported Metformin-Cu(II) Complex as a Recyclable Catalyst

for *N*-arylation of Primary Sulfonamides. *Journal of Organometallic Chemistry*, 948:121915, 2021.

[21] West, M. J., Fyfe, J. W., Vantourout, J. C., and Watson, A. J. Mechanistic Development and Recent Applications of the Chan-Lam Amination. *Chemical Reviews*, 119(24):12491-12523, 2019.

[22] Vijayan, A., Rao, D. N., Radhakrishnan, K. V., Lam, P. Y., and Das, P. Advances in Carbon–Element Bond Construction under Chan-Lam Cross-Coupling Conditions: A Second Decade. *Synthesis*, 53(05):805-847, 2021.

[23] Chen, J. Q., Li, J. H., and Dong, Z. B. A Review on the Latest Progress of Chan-Lam Coupling Reaction. *Advanced Synthesis and Catalysis*, 362(16):3311-3331, 2020.

[24] Yoo, W. J., Tsukamoto, T., and Kobayashi, S. Visible-Light-Mediated Chan-Lam Coupling Reactions of Aryl Boronic Acids and Aniline Derivatives. *Angewandte Chemie International Edition*, 54(22):6587-6590, 2015.

[25] Lam, P. Y. Chan-Lam Coupling Reaction, Copper-Promoted C-Element Bond-Oxidative Coupling Reaction with Boronic Acids, In Blakemore, D. C., Doyle, P. M., Fobian, Y. M., editors, *Synthetic Methods in Drug Discovery*, pages 242-273, The Royal Society of Chemistry, 2016.

[26] Rao, D. N., Rasheed, S., Vishwakarma, R. A., and Das, P. Copper-Catalyzed Sequential *N*-arylation of C-amino-*NH*-azoles. *Chemical Communications*, 50:12911-12914, 2014.

[27] Li, J., Benard, S., Neuville, L., and Zhu, J. Copper Catalyzed *N*-arylation of Amidines with Aryl Boronic Acids and One-Pot Synthesis of Benzimidazoles by a Chan-Lam-Evans *N*-arylation and C-H Activation/C–N Bond Forming Process. *Organic Letters*, 14(23):5980-5983, 2012.

[28] Uemura, T., and Chatani, N. Copper Salt Catalyzed Addition of Arylboronic Acids to Azodicarboxylates. *The Journal of Organic Chemistry*, 70(21):8631-8634, 2005.

[29] Jia, X., and Peng, P. *N*, *O*-Bidentate Ligand-Tunable Copper(II) Complexes as a Catalyst for Chan-Lam Coupling Reactions of Arylboronic Acids with 1*H*-imidazole Derivatives. *Organic & Biomolecular Chemistry*, 16(46):8984-8988, 2018.

[30] Reddy, A. S., Reddy, K. R., Rao, D. N., Jaladanki, C. K., Bharatam, P. V., Lam, P. Y., and Das, P. Copper(II)-Catalyzed Chan-Lam Cross-Coupling: Chemoselective *N*-

arylation of Aminophenols. *Organic & Biomolecular Chemistry*, 15(4):801-806, 2017.

[31] Wang, H., Tu, Y. H., Liu, D. Y., and Hu, X. G. Cu-Catalyzed/Mediated Synthesis of *N*-fluoroalkylanilines from Arylboronic Acids: Fluorine Effect on the Reactivity of Fluoroalkylamines. *Organic & Biomolecular Chemistry*, 16(36):6634-6637, 2018.

[32] Raghuvanshi, D. S., Gupta, A. K., and Singh, K. N. Nickel-Mediated *N*-arylation with Arylboronic Acids: An Avenue to Chan-Lam Coupling. *Organic Letters*, 14(17):4326-4329, 2012.

[33] Hu, G., Chen, W., Fu, T., Peng, Z., Qiao, H., Gao, Y., and Zhao, Y. Nickel-Catalyzed C-P Cross-Coupling of Arylboronic Acids with P(O)H Compounds. *Organic Letters*, 15(20):5362-5365, 2013.

[34] Kumar, K. A., Kannaboina, P., Rao, D. N., and Das, P. Nickel-Catalyzed Chan-Lam Cross-Coupling: Chemoselective *N*-arylation of 2-Aminobenzimidazoles. *Organic & Biomolecular Chemistry*, 14(38):8989-8997, 2016.

[35] Keesara, S. *N*-(Pyridin-2-yl)benzamide: Efficient Ligand for the Nickel Catalyzed Chan-Lam Cross-Coupling Reaction. *Tetrahedron Letters*, 56:6685-6688, 2015.

[36] Dutta, M. M., and Phukan, P. Cu-doped $CoFe_2O_4$ Nanoparticles as Magnetically Recoverable Catalyst for C−N Cross-Coupling Reaction. *Catalysis Communications*, 109:38-42, 2018.

[37] Sharma, C., Sharma, N., Sharma, S., Sharma, S., and Paul, S. Nano-Rod like Morphology of Ni@Fe_3O_4-NDCs on Interaction of NDC-Supported Fe_3O_4 with Nickel NPs: An Efficient Catalyst for Ligand free Chan-Lam Coupling Reaction in Aqueous Medium. *Current Research in Green and Sustainable Chemistry*, 4:100133, 2021.

[38] Kaboudin, B., Abedi, Y., and Yokomatsu, T. One-Pot Synthesis of 1,2,3-Triazoles from Boronic Acids in Water using Cu(II)–β−cyclodextrin Complex as a Nanocatalyst. *Organic & Biomolecular Chemistry*, 10(23):4543-4548, 2012.

[39] Puthiaraj, P., and Pitchumani, K. Triazine-Based Mesoporous Covalent Imine Polymers as Solid Supports for Copper-Mediated Chan-Lam Cross-Coupling *N*-arylation Reactions. *Chemistry–A European Journal*, 20(28):8761-8770, 2014.

[40] Sharma, H., Mahajan, H., Jamwal, B., and Paul, S. Cu@Fe_3O_4-TiO_2-L-Dopa: A Novel and Magnetic Catalyst for the Chan-Lam Cross-Coupling Reaction in Ligand Free Conditions. *Catalysis Communications*, 107:68-73, 2018.

[41] Kumar, A., Layek, S., Agrahari, B., Kujur, S., and Pathak, D. D. Graphene Oxide Immobilized Copper(II) Schiff Base Complex [GO@AF-SB-Cu]: A Versatile Catalyst for Chan-Lam Coupling Reaction. *ChemistrySelect*, 4(4):1337-1345, 2019.

[42] Seyedi, N., Shahabi Nejad, M., Saidi, K., and Sheibani, H. Fabrication of Nitrogen-Enriched Graphene Oxide/Cu NPs as a Highly Efficient and Recyclable Heterogeneous Nanocatalyst for the Chan-Lam Cross-Coupling Reaction. *Applied Organometallic Chemistry*, 34(1):e5307, 2020.

[43] Han, Y., Zhang, M., Zhang, Y. Q., and Zhang, Z. H. Copper Immobilized at a Covalent Organic Framework: An Efficient and Recyclable Heterogeneous Catalyst for the Chan-Lam Coupling Reaction of Aryl Boronic Acids and Amines. *Green Chemistry*, 20(21):4891-4900, 2018.

[44] [a] Xiong, Q. M., Chen, Z., Huang, J. T., Zhang, M., Song, H., Hou, X. F., Li, X. B., and Feng, Z. J. Preparation, Structure and Mechanical Properties of Sialon Ceramics by Transition Metal-Catalyzed Nitriding Reaction. *Rare Metals*, 39(5):589-596, 2020; [b] Shen, Z., Xing, X., Wang, S., Lv, M., Li, J., and Li, T. Effect of K-modified Blue Coke-Based Activated Carbon on Low Temperature Catalytic Performance of Supported Mn−Ce/Activated Carbon. *ACS Omega*, 7(10):8798-8807, 2022; [c] Liu, H., Li, X., Ma, Z., Sun, M., Li, M., Zhang, Z., Zhang, L., Tang, Z., Yao, Y., Huang, B., and Guo, S. Atomically Dispersed Cu-Catalyst for Efficient Chemoselective Hydrogenation Reaction. *Nano Letters*, 21(24):10284-10291, 2021; [d] He, H., Zhu, Q. Q., Yan, Y., Zhang, H. W., Han, Z. Y., Sun, H., Chen, J., Li, C. P., Zhang, Z., and Du, M. Metal-Organic Framework Supported Au-Nanoparticles with Organosilicone Coating for High-Efficiency Electrocatalytic N_2 Reduction to NH_3. *Applied Catalysis B: Environmental*, 302:120840, 2022.

[45] [a] Su, D. S., Zhang, J., Frank, B., Thomas, A., Wang, X., Paraknowitsch, J., and Schlögl, R. Metal-Free Heterogeneous Catalysis for Sustainable Chemistry. *ChemSusChem: Chemistry and Sustainability Energy and Materials*, 3(2):169-180, 2010; [b] Nasri, A., Jaleh, B., Khazalpour, S., Nasrollahzadeh, M., and

Shokouhimehr, M. Facile Synthesis of Graphitic Carbon Nitride/Chitosan/Au Nanocomposite: A Catalyst for Electrochemical Hydrogen Evolution. *International Journal of Biological Macromolecules*, 164:3012-3024, 2020; [c] Besharat, F., Ahmadpoor, F., Nezafat, Z., Nasrollahzadeh, M., Manwar, N. R., Fornasiero, P., and Gawande, M. B. Advances in Carbon Nitride-Based Materials and Their Electrocatalytic Applications. *ACS Catalysis*, 12:5605-5660, 2022.

[46] Wang, Y., Wang, X., and Antonietti, M. Polymeric Graphitic Carbon Nitride as a Heterogeneous Organocatalyst: from Photochemistry to Multipurpose Catalysis to Sustainable Chemistry. *Angewandte Chemie International Edition*, 51(1):68-89, 2012.

[47] Su, F., Antonietti, M., and Wang, X. mpg-C_3N_4 as a Solid Base Catalyst for Knoevenagel Condensations and Transesterification Reactions. *Catalysis Science and Technology*, 2(5):1005-1009, 2012.

[48] Choudhary, P., Bahuguna, A., Kumar, A., Dhankhar, S. S., Nagaraja, C. M., and Krishnan, V. Oxidized Graphitic Carbon Nitride as a Sustainable Metal-Free Catalyst for Hydrogen Transfer Reactions Under Mild Conditions. *Green Chemistry*, 22(15):5084-5095, 2020.

[49] Kang, S., He, M., Chen, M., Wang, J., Zheng, L., Chang, X., Duan, H., Sun, D., Dong, M., and Cui, L. Ultrafast Plasma Immersion Strategy for Rational Modulation of Oxygen-Containing and Amino Groups in Graphitic Carbon Nitride. *Carbon*, 159:51-64, 2020.

[50] [a] Zhang, S., Li, J., Zeng, M., Zhao, G., Xu, J., Hu, W., and Wang, X. *In situ* Synthesis of Water-Soluble Magnetic Graphitic Carbon Nitride Photocatalyst and its Synergistic Catalytic Performance. *ACS Applied Materials and Interfaces*, 5(23):12735-12743, 2013; [b] Li, H. J., Sun, B. W., Sui, L., Qian, D. J., and Chen, M. Preparation of Water-Dispersible Porous g-C_3N_4 with Improved Photo-catalytic Activity by Chemical Oxidation. *Physical Chemistry Chemical Physics*, 17(5):3309-3315, 2015.

[51] Kumar, R., Barakat, M. A., and Alseroury, F. A. Oxidized g-C_3N_4/Polyaniline Nanofiber Composite for the Selective Removal of Hexavalent Chromium. *Scientific Reports*, 7(1):1-11, 2017.

[52] Zhong, R., Zhang, Z., Yi, H., Zeng, L., Tang, C., Huang, L., and Gu, M. Covalently Bonded 2D/2D O-g-C_3N_4/TiO_2 Heterojunction for Enhanced Visible-Light Photocatalytic Hydrogen Evolution. *Applied Catalysis B: Environmental*, 237:1130-1138, 2018.

[53] Wang, X., Maeda, K., Thomas, A., Takanabe, K., Xin, G., Carlsson, J. M., Domen, K., and Antonietti, M. A Metal-Free Polymeric Photocatalyst for Hydrogen Production from Water Under Visible Light. *Nature Materials*, 8(1):76-80, 2009.

[54] Qiu, P., Xu, C., Chen, H., Jiang, F., Wang, X., Lu, R., and Zhang, X. One Step Synthesis of Oxygen Doped Porous Graphitic Carbon Nitride with Remarkable Improvement of Photo-Oxidation Activity: Role of Oxygen on Visible Light Photocatalytic Activity. *Applied Catalysis B: Environmental*, 206:319-327, 2017.

[55] [a] Xu, J., Wu, H. T., Wang, X., Xue, B., Li, Y. X., and Cao, Y. A New and Environmentally Benign Precursor for the Synthesis of Mesoporous g-C_3N_4 with Tunable Surface Area. *Physical Chemistry Chemical Physics*, 15(13):4510-4517, 2013; [b] Dutta, G. K., and Karak, N. Bio-Based Waterborne Polyester Supported Oxygeneous Graphitic Carbon Nitride Nanosheets as a Sustainable Photo-catalyst for Aquatic Environment Remediation. *Journal of Cleaner Production*, 285:124906, 2021.

[56] Loupy, A. Solvent-Free Microwave Organic Synthesis as an Efficient Procedure for Green Chemistry. *Comptes Rendus Chimie*, 7(2):103-112, 2004.

[57] Kharlamov, A., Bondarenko, M., Kharlamova, G., and Gubareni, N. Features of the Synthesis of Carbon Nitride Oxide (g-C_3N_4)O at urea pyrolysis. *Diamond and Related Materials*, 66:16-22, 2016.

[58] Smýkalová, A., Foniok, K., Cvejn, D., Górecki, K. M., and Praus, P. The Role of Guanidine Hydrochloride in Graphitic Carbon Nitride Synthesis. *Scientific Reports*, 11(1):1-18, 2021.

[59] Wang, H., Jiang, S., Chen, S., Li, D., Zhang, X., Shao, W., Sun, X., Xie, J., Zhao, Z., Zhang, Q., Tian, Y., and Xie, Y. Enhanced Singlet Oxygen Generation in Oxidized Graphitic Carbon Nitride for Organic Synthesis. *Advanced Materials*, 28(32):6940-6945, 2016.

[60] Dong, J., Zhao, Y., Chen, H., Liu, L., Zhang, W., Sun, B., Yang, M., Wang, Y., and Dong, L. Fabrication of PEGylated Graphitic Carbon Nitride Quantum Dots as Traceable, pH-Sensitive Drug Delivery Systems. *New Journal of Chemistry*, 42(17):14263-14270, 2018.

[61] [a] Koiki, B. A., Orimolade, B. O., Peleyeju, G. M., and Arotiba, O. A. Rapid and Template-Free Synthesis of Copper(I) Oxide-Graphitic Carbon Nitride Hetero-junction for Photocatalytic Degradation of Orange II Dye in Water. *Solid State Sciences*, 97:105994, 2019; [b] Kumar, A., Kumar, P., Joshi, C., Manchanda, M., Boukherroub, R., and Jain, S. L. Nickel Decorated on Phosphorous-Doped Carbon Nitride as an Efficient Photocatalyst for Reduction of Nitrobenzenes. *Nanomaterials*, 6(4):59, 2016.

[62] Celep, G., Cottancin, E., Lermé, J., Pellarin, M., Arnaud, L., Huntzinger, J. R., Vialle, J. L., Broyer, M., Palpant, B., Boisron, O., and Mélinon, P. Optical Properties of Copper Clusters Embedded in Alumina: An Experimental and Theoretical Study of Size Dependence. *Physical Review B*, 70(16):165409, 2004.

[63] Kim, Y. H., Lee, D. K., Cha, H. G., Kim, C. W., Kang, Y. C., and Kang, Y. S. Preparation and Characterization of the Antibacterial Cu Nanoparticle Formed on the Surface of SiO_2 Nanoparticles. *The Journal of Physical Chemistry B*, 110(49):24923-24928, 2006.

[64] Gong, Y., Li, M., Li, H., and Wang, Y. Graphitic Carbon Nitride Polymers: Promising Catalysts or Catalyst Supports for Heterogeneous Oxidation and Hydrogenation. *Green Chemistry*, 17(2):715-736, 2015.

[65] Zhu, J., Xiao, P., Li, H., and Carabineiro, S. A. Graphitic Carbon Nitride: Synthesis, Properties, and Applications in Catalysis. *ACS Applied Materials and Interfaces*, 6(19):16449-16465, 2014.

[66] Chen, C. S., Chen, C. C., Chen, C. T., and Kao, H. M. Synthesis of Cu Nanoparticles in Mesoporous Silica SBA-15 Functionalized with Carboxylic Acid Groups. *Chemical Communications*, 47(8):2288-2290, 2011.

[67] Han, Q., Wang, B., Gao, J., Cheng, Z., Zhao, Y., Zhang, Z., and Qu, L. Atomically Thin Mesoporous Nanomesh of Graphitic C_3N_4 for High-Efficiency Photocatalytic Hydrogen Evolution. *ACS Nano*, 10(2):2745-2751, 2016.

[68] [a] Thomas, A., Fischer, A., Goettmann, F., Antonietti, M., Müller, J. O., Schlögl, R., and Carlsson, J. M. Graphitic Carbon Nitride Materials: Variation of Structure and Morphology and their Use as Metal-Free Catalysts. *Journal of Materials Chemistry*, 18(41):4893-4908, 2008; [b] Cui, Y., Ding, Z., Fu, X., and Wang, X. Construction of Conjugated Carbon Nitride Nanoarchitectures in Solution at Low Temperatures for Photo-redox Catalysis. *Angewandte Chemie International Edition*, 51(47):11814-11818, 2012.

[69] [a] Popok, V. N., Novikov, S. M., Lebedinskij, Y. Y., Markeev, A. M., Andreev, A. A., Trunkin, I. N., Arsenin, V. A., and Volkov, V. S. Gas-Aggregated Copper Nanoparticles with Long-Term Plasmon Resonance Stability. *Plasmonics*, 16(2):333-340, 2021; [b] Zhang, R., Hu, L., Bao, S., Li, R., Gao, L., Li, R., and Chen, Q. Surface Polarization Enhancement: High Catalytic Performance of Cu/CuOx/C Nanocomposites Derived from Cu-BTC for CO Oxidation. *Journal of Materials Chemistry A*, 4(21):8412-8420, 2016.

[70] Raul, P. K., Mahanta, A., Bora, U., Thakur, A. J., and Veer, V. In Water Homocoupling of Arylboronic Acids Using Nano-Rod Shaped and Reusable Copper Oxide(II) Catalyst at Room Temperature. *Tetrahedron Letters*, 56(51):7069-7073, 2015.

[71] Camats, M., Pla, D., and Gómez, M. Copper Nanocatalysts Applied in Coupling Reactions: A Mechanistic Insight. *Nanoscale*, 13(45):18817-18838, 2021.

[72] Nandi, D., Taher, A., Ul Islam, R., Siwal, S., Choudhary, M., and Mallick, K. Carbon Nitride Supported Copper Nanoparticles: Light-Induced Electronic Effect of the Support for Triazole Synthesis. *Royal Society Open Science*, 3(11):160580 (1-11), 2016.

[73] Tromp, M., van Strijdonck, G. P., van Berkel, S. S., van den Hoogenband, A., Feiters, M. C., de Bruin, B., Fiddy, S. G., van der Eerden, A. M. J., van Bokhoven, J. A., van Leeuwen, P. W. N. M., Koningsberger, D. C Multi-technique Approach to Reveal the Mechanism of Copper(II)-Catalyzed Arylation Reactions. *Organometallics*, 29(14):3085-3097, 2010.

[74] Smith, G. B., Dezeny, G. C., Hughes, D. L., King, A. O., and Verhoeven, T. R. Mechanistic Studies of the Suzuki Cross-Coupling Reaction. *The Journal of Organic Chemistry*, 59(26):8151-8156, 1994.

[75] Candeias, N. R., Cal, P. M., Andre, V., Duarte, M. T., Veiros, L. F., and Gois, P. M. Water as the Reaction Medium for Multi-component Reactions Based on Boronic Acids. *Tetrahedron*, 66(14):2736-2745, 2010.

[76] Huffman, L. M., and Stahl, S. S. Carbon-Nitrogen Bond Formation Involving Well-Defined Aryl-Copper(III) Complexes. *Journal of the American Chemical Society*, 130(29):9196-9197, 2008.

[77] Ribeiro, F. H., Schach von Wittenau, A. E., Bartholomew, C. H., Somorjai, G. A. Reproducibility of Turnover Rates in Heterogeneous Metal Catalysis: Compilation of Data and Guidelines for Data Analysis. *Catalysis Reviews*, 39(1-2):49-76, 1997.

[78] Boudart, M. Turnover Rates in Heterogeneous Catalysis. *Chemical Reviews*, 95(3):661-666, 1995.

[79] Kozuch, S., and Martin, J. M. "Turning Over" Definitions in Catalytic Cycles. *ACS Catalysis*, 2(12):2787-2794, 2012.

[80] Lan, J. B., Chen, L., Yu, X. Q., You, J. S., and Xie, R. G. A Simple Copper Salt Catalyzed the Coupling of Imidazole with Arylboronic Acids in Protic Solvent. *Chemical Communications*, (2):188-189, 2004.

[81] Kantam, M. L., Venkanna, G. T., Sridhar, C., Sreedhar, B., and Choudary, B. M. An Efficient Base-Free *N*-arylation of Imidazoles and Amines with Arylboronic Acids Using Copper-Exchanged Fluorapatite. *The Journal of Organic Chemistry*, 71(25):9522-9524, 2006.

[82] Old, D. W., Harris, M. C., and Buchwald, S. L. Efficient Palladium-Catalyzed *N*-arylation of Indoles. *Organic Letters*, 2(10):1403-1406, 2000.

[83] Bordwell, F. G. Equilibrium Acidities of Carbon Acids, In Fruchier, A., editor, *Physical Organic Chemistry-3*, pages 963-968, Pergamon Press, 1977.

[84] Yagil, G. The Proton Dissociation Constant of Pyrrole, Indole and Related Compounds. *Tetrahedron*, 23(6):2855-2861, 1967.

[85] Urgaonkar, S., and Verkade, J. G. Scope and Limitations of $Pd_2(dba)_3$/P(*i*-$BuNCH_2CH_2)_3N$-Catalyzed Buchwald-Hartwig Amination Reactions of Aryl Chlorides. *The Journal of Organic Chemistry*, 69(26):9135-9142, 2004.

[86] Song, H., Shen, Y., Zhou, H., Ding, D., Yang, F., Wang, Y., Xu, C., and Cai, X. Light-Promoted Low-Valent-Tungsten-Catalyzed Ambient Temperature Amination of Boronic Acids with Nitroaromatics. *The Journal of Organic Chemistry*, 87(8):5303-5314, 2022.

[87] Guo, X., Rao, H., Fu, H., Jiang, Y., and Zhao, Y. An Inexpensive and Efficient Copper Catalyst for *N*-Arylation of Amines, Amides and Nitrogen-Containing Heterocycles. *Advanced Synthesis & Catalysis*, 348(15):2197-2202, 2006.

[88] Ando, S., Hirota, Y., Matsunaga, H., and Ishizuka, T. Nickel-catalyzed *N*-arylation of Amines with Arylboronic Acids Under Open Air. *Tetrahedron Letters*, 60(18):1277-1280, 2019.

[89] Yang, C. T., Fu, Y., Huang, Y. B., Yi, J., Guo, Q. X., and Liu, L. Room-Temperature Copper-Catalyzed Carbon-Nitrogen Coupling of Aryl Iodides and Bromides Promoted by Organic Ionic Bases. *Angewandte Chemie International Edition*, 48(40):7398-7401, 2009.

[90] Di, J. Q., Zhang, M., Chen, Y. X., Wang, J. X., Geng, S. S., Tang, J. Q., and Zhang, Z. H. Copper Anchored on Phosphorus g-C_3N_4 as a Highly Efficient Photocatalyst for the Synthesis of *N*−arylpyridin-2-amines. *Green Chemistry*, 23(2):1041-1049, 2021.

[91] Sarmah, M., Dewan, A., Boruah, P. K., Das, M. R., and Bora, U. Intercalation of Copper Salt to Montmorillonite K-10 and its Application as a Reusable Catalyst for Chan-Lam Cross-Coupling Reaction. *Applied Organometallic Chemistry*, 34(4):e5554, 2020.

[92] Kiyomori, A., Marcoux, J. F., and Buchwald, S. L. An Efficient Copper-Catalyzed Coupling of Aryl Halides with Imidazoles. *Tetrahedron Letters*, 40(14):2657-2660, 1999.

[93] Altman, R. A., Koval, E. D., and Buchwald, S. L. Copper-Catalyzed *N*-arylation of Imidazoles and Benzimidazoles. *The Journal of Organic Chemistry*, 72(16):6190-6199, 2007.

[94] Duveau, D. Y., Hu, X., Walsh, M. J., Shukla, S., Skoumbourdis, A. P., Boxer, M. B., Ambudkar, S. V., Shen, M., and Thomas, C. J. Synthesis and Biological Evaluation of Analogues of the Kinase Inhibitor Nilotinib as Abl and Kit Inhibitors. *Bioorganic and Medicinal Chemistry Letters*, 23(3):682-686, 2013.

[95] Fevig, J. M., Pinto, D. J., Han, Q., Quan, M. L., Pruitt, J. R., Jacobson, I. C., Galemmo, R. A., Wang, J. S., Orwat, M. J., Bostrom, L. L., Knabb, R. M., Wong, P. C., Lam, P. Y. S., and Wexler, R. R. Synthesis and SAR of Benzamidine Factor Xa Inhibitors Containing a Vicinally-Substituted Heterocyclic Core. *Bioorganic and Medicinal Chemistry Letters*, 11(5):641-645, 2001.

[96] Siddiqui, I. R., Ibad, F., Ibad, A., Waseem, M. A., and Watal, G. Eco-Friendly Strategy: Design and Synthesis of Biologically Potent Benzimidazole-Amine Hybrids *via* Visible-Light Generated Oxidative C−H Arylamylation of Analenic Amidines. *Tetrahedron Letters*, 57(1):5-10, 2016.

[97] Malavade, V., Patil, M., and Patil, M. Scope, Kinetics, and Mechanism of "On Water" Cu Catalysis in the C−N Cross-Coupling Reactions of Indole Derivatives. *European Journal of Organic Chemistry*, 2020(5):561-569, 2020.

[98] Chen, X., Lin, J., Wang, B., and Tian, X. Nickel-Catalyzed Mizoroki-Heck/Amination Cascade Reactions of *o*-Dihaloarenes with Allylamines: Synthesis of Indoles. *Organic Letters*, 22(19):7704-7708, 2020.

[99] Ge, X., Zhang, S., Chen, X., Liu, X., and Qian, C. A Designed Bi-Functional Sugar-Based Surfactant: Micellar Catalysis for C−X Coupling Reaction in Water. *Green Chemistry*, 21(10):2771-2776, 2019.

[100] Pawar, G. G., Wu, H., De, S., and Ma, D. Copper(I) Oxide/*N*,*N'*-bis [(2-furyl)methyl]oxalamide-Catalyzed Coupling of (Hetero)aryl Halides and Nitrogen Heterocycles at Low Catalytic Loading. *Advanced Synthesis & Catalysis*, 359(10):1631-1636, 2017.

[101] He, F., and Wang, Z. X. Nickel-Catalyzed Cross-Coupling of Aryl or 2-Menaphthyl Quaternary Ammonium Triflates with Organoaluminum Reagents. *Tetrahedron*, 73(30):4450-4457, 2017.